TALLINNA TEHNIKAÜLIKOOL
EHITUSTEADUSKOND
EHITISTE PROJEKTEERIMISE INSTITUUT

TESTING OF GLULAM BEAMS IN FIRE WITH SPECIFIC LOCAL MATERIAL PROPERTIES

LIIMPUITTALADE KATSELINE UURIMINE MATERJALI KOHALIKE OMADUSTE MÕJU MÄÄRAMISEKS TULEKAHJUOLUKORRAS

EEK 60 LT

Üliõpilane: **Andres Ollino**

....

Juhendaja: **Dots. Alar Just**

Michael Klippel

....

Tallinn, 2016

Olen koostanud lõputöö iseseisvalt.

Kõik töö koostamisel kasutatud teiste autorite

tööd, olulised seisukohad, kirjandusallikatest ja mujalt

pärinevad andmed on viidatud.

…………………………………………….. (töö autori allkiri ja kuupäev)

Üliõpilase kood:

162396EAEI

Töö vastab magistritööle esitatud nõuetele.

…………………………………………… (juhendaja allkiri ja kuupäev)

Kaitsmisele lubatud ………………………….. (kuupäev)

Kaitsmiskomisjoni esimees ………………………….. (allkiri)

LÕPUTÖÖ ÜLESANNE

Üliõpilase kood	**162396EAEI**
Ehitustehnika õppesuuna üliõpilasele	**ANDRES OLLINO**
Lõputöö kood:	**EEK 60LT**
Lõputöö juhendaja:	**ALAR JUST**
Lõputöö kaasjuhendaja:	**MICHAEL KLIPPEL (ETH)**
Lõputöö teema:	

TESTING OF GLULAM BEAMS IN FIRE WITH SPECIFIC LOCAL MATERIAL PROPERTIES

Liimpuittalade katseline uurimine materjali kohalike omaduste mõju määramiseks tulekahjuolukorras

Lõputöö teema kehtivusaeg: **31.12.2016**

Lõputöö ülesanne:

Teostada koormuse all tulekatsed hästi teada olevate kohalike materjaliomadustega liimpuittaladega . Dokumenteerida talade omadused enne tulekatseid, nende ajal ning pärast katsetamist.

Lõputöö sisu:

ETH Zürich on valmistanud 6 liimpuittala, mille lamellide tugevusomadused on detailselt teada. Nimetatud talade tugevust mõjutavad näitajad (tihedus, sõrmjätkud, niiskusesisaldus, võimalik pragude esinemine jm) tuleb detailselt mõõta ja dokumenteerida. Seejärel tuleb nende taladega teostada koormuse all tulekatsed ning tulemusi analüüsida.

Töö tulemuseks on alusmaterjal simulatsiooniprogrammi jaoks, millega leitakse puitkonstruktsioonide tugevusnäitajate normaaljaotust kõrgetel temperatuuridel.

Töö kirjutada inglise keeles.

Resümee eesti keeles

Lõputöö konsultandid:

Töö osa nimetus	Konsultandi nimi	Konsultandi allkiri	Kuupäev

Lõputöö väljaandmise kuupäev: **20.09.2015**

Juhendaja: **Alar Just** ……………………..

Ülesande vastu võtnud: **Andres Ollino** ....

4

Contents

1 Introduction

1.1 General

Throughout the history, wood has been used for several kinds of building constructions. Wood has a remarkably high strength to weight ratio, and thermal properties, aesthetically valued, is durable, if maintained with care. Wood can be easily shaped, is reachable, is growing on its own and is renewable.

The usage of wooden constructions has increased over the last decades, concerning not only small residential houses but also public and industrial buildings. In contemporary wooden structures Glued Laminated Timber (glulam or GLT) plays an important role. Research and development processes have allowed the implementation of variety of new materials over time of which Cross Laminated Timber (CLT) and composite constructions using glulam have strongly boosted ambitions of wooden multi-storey buildings. Fire safety requirements obtain relatively higher importance in structural design of tall buildings. With deviation of properties and combustibility of timber added, finding solutions for safe exploitation is challenging. The research of this thesis gives its small contribution to the fire safe future of so-called green buildings.

1.2 The aim of this thesis

In 2014, Fink [1] developed a probabilistic approach for modelling glulam beams. Although several models have been presented over time, Fink developed his model to use data from contemporary timber board grading device. Motivation of the current work is to test and analyse the fire resistance of the glulam beams with well-known local material properties based on the work of Fink [1] to provide an input for the further development of the research on the design of timber members in fire.

1.3 Acknowledgements

2 Previous studies

2.1 Strength properties of timber in normal conditions.

Madsen et al. [4] have phrased an important aspect of structural timber - The two products - wood, in the sense of clear defect-free wood and timber, in the sense of commercial timber - have to be considered as two different materials and that must be respected when strength properties are developed for engineering purposes.

Unlike man-made materials, such as steel and concrete, timber is a natural grown material. Therefore, it is heterogeneous in structure and anisotropic. High variability of properties appears not only between different structural elements but also within single elements. The variability between timber elements is presented in Figure 1. It can be noticed in the chart that bending strength between members with the same global modulus of elasticity may differ up to four times or more.
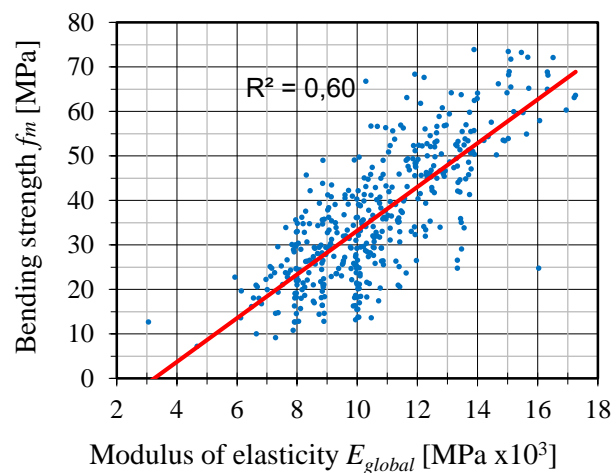

Figure 1. Bending strength versus modulus of elasticity of ~400 timber boards. Data taken from [5]

To describe the mechanical performance of structural timber components both; (a) the material properties of clear defect-free timber, and (b) the influence of growth irregularities have to be considered.

9

The material properties of timber for engineering are described as parallel to the grain and perpendicular to the grain. Clear defect-free timber can be described using an orthotropic material behaviour having three main axes: longitudinal, radial and tangential [1] [6]. The results of studies [7] show that the strength and stiffness properties in longitudinal direction are significantly larger than in radial and tangential directions, which are relatively similar.

Timber boards are sawn out of a trunk of the tree rather parallel to its longitudinal axis and grain orientation is assumed to be parallel as well. As timber is natural grown, grain orientation may deviate globally due to the spiral grain angle, described by Harris [8], or locally because of knots or knot clusters. For Norway spruce specimens the magnitude of the spiral grain angles has been found to vary in general between zero and five degrees. The strength and stiffness properties are about 15 - 20% lower for a timber board with a spiral grain angle of four degrees compared to a timber board with no spiral grain angle [9], [10], [11]. Local changes in grain orientation around knots, especially considering sawing patterns, may result in significantly lower strength properties of a single board. Some knot arrangements within a timber board is illustrated in Figure 2.
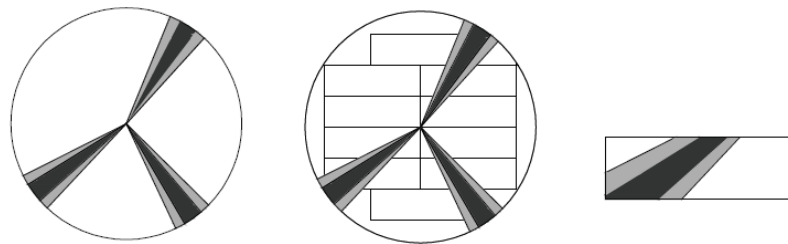
Figure 2. Knot arrangement in a solid timber board. [12]
(left) knot arrangement within the cross-section of a tree trunk, (middle) influence of the sawing pattern on the knot distribution within sawn timber boards, and (right) resulting knot area within the cross-section of one timber board.

Due to the occurrence of growth irregularities, the material properties of structural timber components are significantly lower, compared to the material properties of clear defect-free timber.

Glulam is a structural product of several layers of timber boards glued together. Compared to solid timber, glulam has several advantages, of which lower deviation in properties and noticeably larger range of dimensions to choose from are two of most important ones.

Glulam beams are fabricated of graded timber beams, usually with thickness of 30-50mm. First endless lamellas are produced by connecting timber boards using finger joints (FJ). Lamellas are then planed and cut into the required length and glued together. As final step the new beam is planed and given final shape. Illustration from Fink is presented in Figure 3.

Fink [1] has characterised the performance of a glulam element as follows: the mechanical performance of glulam beams can be described as a combined performance of its single components. That includes the mechanical performance of timber boards, FJ and glue-lines between the timber boards. Further, the arrangement of timber boards and FJ within the glulam beams has to be considered.
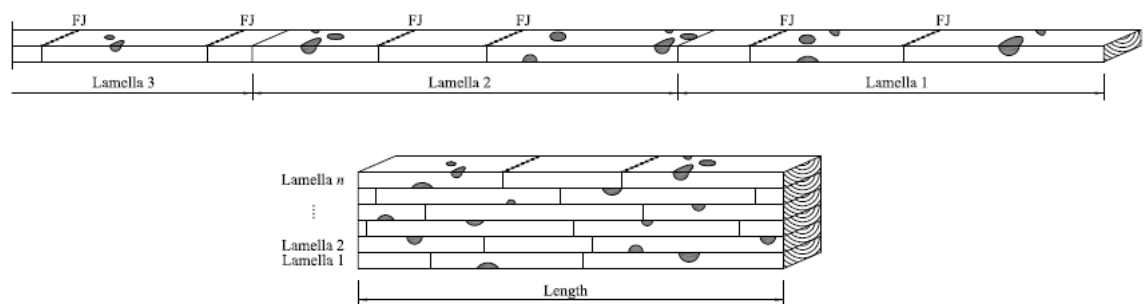
Figure 3. Fabrication of Glulam beams. [1]

In the following, some aspects of the mechanical performance of glulam are explained further; abbreviated from Fink [1].

Within a glulam beam having numerous lamellas, the bending stress within lamellas can be approximated with the normal stresses within the lamellas. However, in general, the bending capacity of glulam beams exceeds the tensile capacity of the lamellas, mostly due to the lamination effect. The lamination effect is explained in numerous of publications of Falk & Colling [13], Serrano & Larsen [14]. Shortened, the ideas would be that the defects

of single lamellas are more evenly distributed, local weak sections, such as knot clusters or FJ are reinforced by adjacent lamellas and contemporary centrically loaded testing procedures adjacent lamellas prevent lateral bending.

Similarly to knot clusters, also finger joint connections can be considered as local weak sections within glulam beams. In general, the load bearing capacity of FJ is significantly smaller than that of the adjacent clear wood, whereas the stiffness is comparable [15], [16]. According to Colling [17] the tensile strength of FJ can be assumed to be similar to the tensile strength of a knot cluster with tKAR = 0:25 - 0,30 (for tKAR please see Section 4.1). Due to the relatively large stiffness FJ attract higher stresses, compared to knot clusters [18] investigated 115 glulam beams. The investigation showed that the amount of failures related to FJ increases with increasing timber quality. Further, it seems that the probability of a FJ-failure decreases with increasing glulam dimensions.

2.2   Strength properties of timber in fire conditions.

Unfortunately, only very few test results exist on timber members exposed to fire where the 'cold' strength properties were predicted with sufficient accuracy, which makes it difficult to compare calculation models with test results. A report Joakim Norén [1] presented at the International Conference on Timber Engineering in Seattle in 1988 of research to investigate the behaviour of loaded structural timber elements when exposed to fire, can be introduced as an exception. Norén performed loaded bending tests with four groups of solid wood beams of dimensions 45x120x2300 mm of high and low strength grades, about 20 specimens in each group. In order to evaluate the effect of being exposed to fire to the strength properties, carefully matched (including matching or symmetrical cutting of knots) pairs of specimens were chosen. First, bending stiffness in normal condition of all specimens was determined. Then bending strength of one specimen of the pair was tested in normal conditions and the other one, loaded with 1/3 or 1/6 of the ultimate moment in normal conditions, was tested until failure in fire. The most significant findings were that the loss of load bearing capacity involves in addition to charring of wood also temperature-dependent reduction of strength and stiffness of the uncharred residual cross-section. Presented in Figure 4.
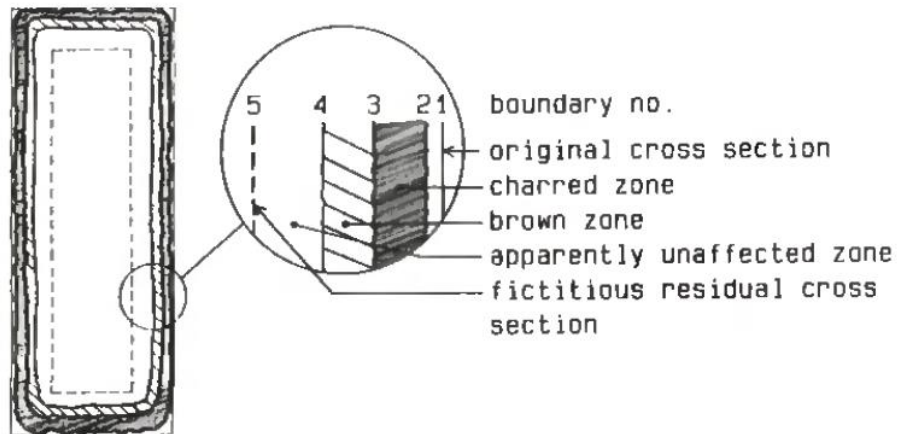
Figure 4. Cross-section of timber after being exposed to fire by Norén. [1]

In the current version of Eurocode 5 (EC5) Part 1-2 [2] apparently unaffected cross-section together with the brown zone in Figure 4 is called zero strength layer d_0 and the thickness of it is still debated.

Norén also compared the distribution of the calculated bending strength in normal conditions and in fire. From the tests, a decrease of the scatter in the fire situation was observed (see Figure 5); however, this fact was not the main reason of the decision of using 20% fractile values.

13
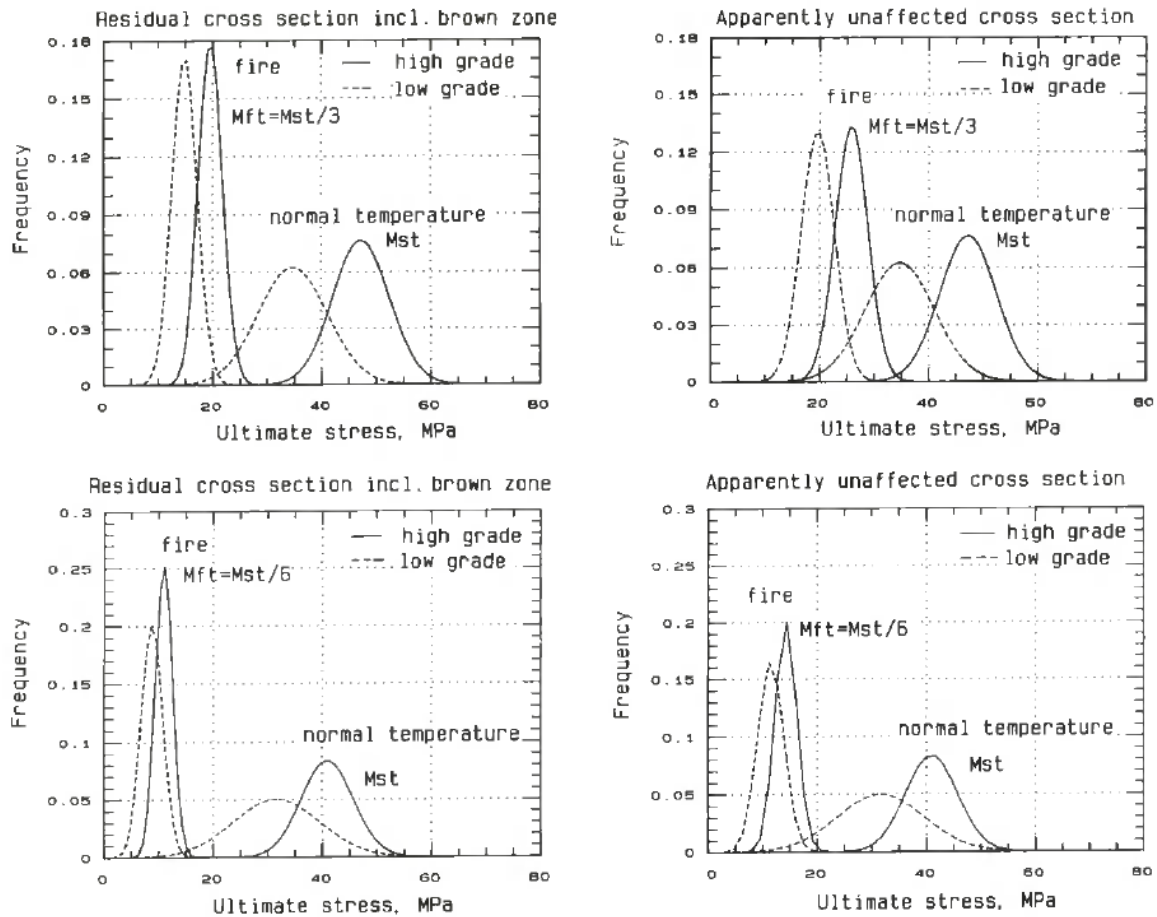
Figure 5. Fitted normal frequency curves for bending strength, under fire exposure conditions ant at normal temperature, of high grade timber (solid curves) and low grade timber (dashed curves). The bending strength is calculated on the residual cross-section including the brown zone (to the left) and on the apparently unaffected cross-section (to the right) respectively. Image and caption [1]

Considering the bonding materials used for production of the specimens of this study (please see Section 4.2), performance of glues in fire must not be overlooked. Klippel [21] investigated the fire resistance of finger joints bonded with different types of glues and different products available within the type. Novel adhesives have been put on the market. These adhesives are cheaper, permit shorter hardening times (in the case of melamine-(urea)-formaldehyde adhesives, MF/MUF) and, in the case of polyurethane (PUR) adhesives, are also free from formaldehyde. The thermal stability of these adhesives in glued engineered wood products has been one of their key criteria, since the mechanical

14

performance of these novel adhesives declines with increasing temperature. Hence, using such adhesives in bonded wood joints might lead to a lower resistance in the case of fire of the engineered wood product.

In Section 5.5.2 the depth of zero strength layer for specimens is calculated. The concept is illustrated by Klippel [21]. The illustration is presented in Figure 6.

Concept of Reduced cross-section method

Equal load resistance at fire exposure $M_{R,fi}$ calculated for:

Residual cross-section with $f = f_m(T)$ Effective cross-section with $f = f_{20°C}$

Residual cross-section

equivalent

Effective cross-section

$d_{char,n}$
$k_0 d_0$
d_{ef}

$M_{R,fi} = W_{fi,advanced} \cdot f_m(T)$ Difference: Zero strength layer d_0 $M_{R,fi} = W_{fi,effective} \cdot f_{20°C}$
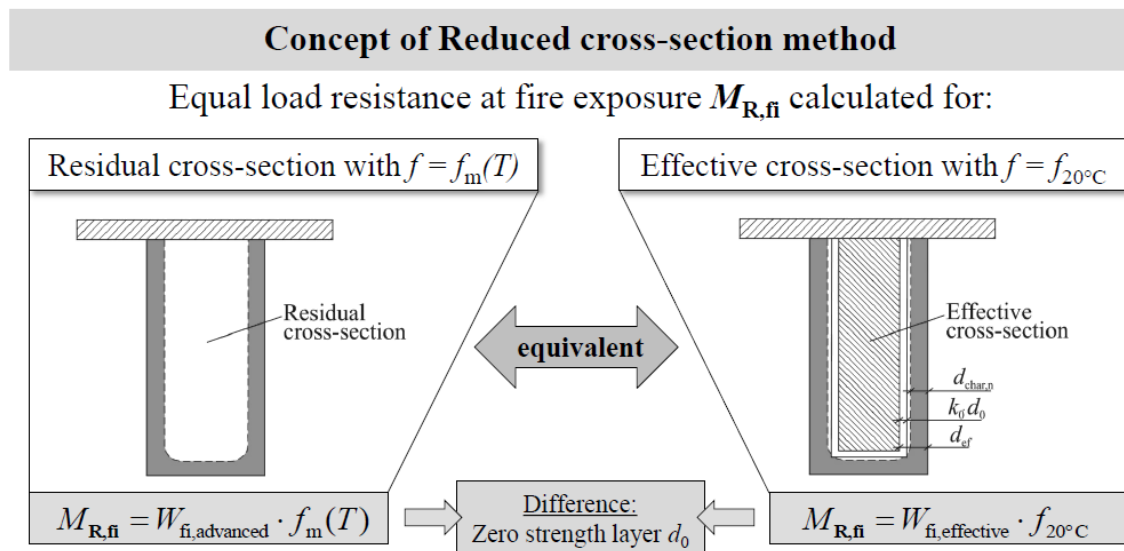
where

$M_{R,fi}$	is the load resistance at fire exposure
$W_{fi,advanced}$	is the section modulus of the residual cross-section determined with a heat transfer analysis using Annex B of EN 1995-1-2 (2004)
$f_m(T)$	is the temperature-dependent bending strength
$W_{fi,effective}$	is the section modulus of the effective cross-section
$f_{20°C}$	is the bending strength at normal temperature

Figure 6. Concept of Reduced cross-section method; zero-strength layer explained, adapted from Klippel [21].

Analysis of the depth of zero-strength layer can be found in Klippel [21].

Further, performed zero-strength layer investigations before 2012 is are summarised by Schmid et. al. [22].

3 Fire resistance of timber structures by Eurocode 5

In this Section, important aspects of the fire resistance of loaded timber members are introduced.

According to the current version of Eurocode 5 Part 1-2 [2], timber elements must meet the requirement of maintaining their load bearing function during the relevant time of fire exposure. Two different approaches are provided for fire design: The "Reduced cross-section method" (RCSM) and the "Reduced properties method" [19]. The latter will not be covered further in this thesis. The "Reduced cross-section method" permits the designer to use strength and stiffness properties for normal temperature for the residual effective cross-section. [Note: That is also the reason why the "Reduced cross-section method will most probably be renamed to "Effective cross-section" in the new Eurocode 5]

EC5 Part 1-2 [2] determines one-dimensional charring rate for a semi-infinite softwood slab exposed to ISO 834 [20] fire of β_0=0,65mm/min. For designing rectangular elements, considering the roundings of the corners due to the two-dimensional heat flux, a simplification of an equivalent rectangular residual cross-section assuming a higher charring rate is provided. For glued laminated timber charring rate, which considers the roundings and is called notional charring rate, is given β_n=0,7mm/min. The depth of charring is calculated multiplying the time of fire exposure by charring rate. Besides charring, using RCSM cross-section is lessened additionally due to the temperature-dependent reduction of strength properties close to the charring line. Dimensions are reduced by the thickness of zero-strength layer $k_0 \times d_0$. The result is called an effective cross-section, and in fire design for this cross-section strength properties of timber in normal temperature can be applied. Effective cross-section is explained in Figure 7 and in Figure 8.
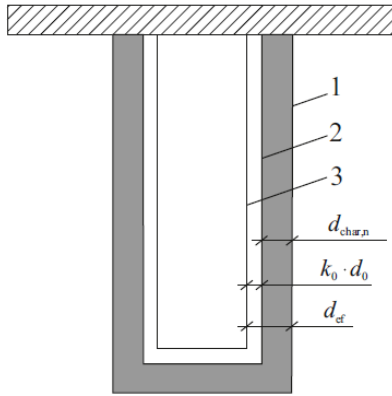
Key:
1 Initial surface of member
2 Border of residual cross-section
3 Border of effective cross-section

$d_{char,n}$ is the notional charring depth
d_0 is the zero-strength layer: $d_0 = 7mm$
k_0 $k_0 = 1.0$ for t $\geq$ 20 minutes
$k_0 = t/20$ for t < 20 minutes
t is the time of fire exposure
d_{ef} is the effective charring depth

Figure 7. Definition of residual and effective cross-section; further information is given by König [19], adapted from Klippel [21].
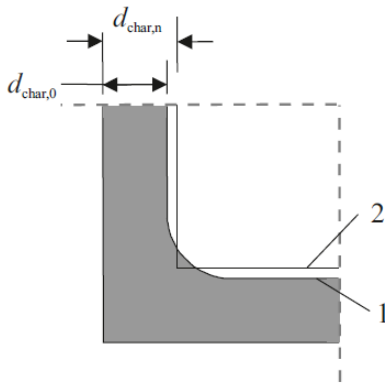
Key:
1 Residual cross-section
2 Equivalent, rectangular residual cross-section

$d_{char,0}$ is the one-dimensional charring depth
$d_{char,n}$ is the notional charring depth

Figure 8. The one-dimensional charring depth d$_{char,0}$ and the corner roundings are replaced with an equivalent (notional) charring depth d$_{char,n}$; ; further information is given by König [19], adapted from Klippel [21].

The strength value to calculate the fire resistance $R_{d,fi}$ is determined by current version of Eurocode 5 Part 1-2 [2] as follows:

$$f_{d,fi} = k_{mod,fi} \times \frac{f_{20}}{\gamma_{M,fi}} = k_{mod,fi} \times \frac{k_{fi} \times f_k}{\gamma_{M,fi}}$$

where

$f_{d,fi}$ is the design strength of timber in fire, e.g. bending strength

17

f_k	is the 5% fractile characteristic strength properties of timber (bending strength, tensile strength, shear strength, etc.) at normal temperature depending on the strength class according to EN 338 [23]
f_{20}	is the 20% fractile of the strength property
k_{fi}	is the modification factor for fire, taking into account the 20% fractiles of strength properties of timber ($f_{20}=k_{fi}\times f_k$) $k_{fi}=1,25$ for solid timber $k_{fi}=1,15$ for glued laminated timber
$k_{mod,fi}$	is the modification factor for fire taking into account the effects of temperature on the strength properties of timber
$\gamma_{M,fi}$	Is the partial safety factor for timber in fire ($\gamma_{M,fi}=1,0$)

According to Eurocode 5 Part 1-2 [2] the dimensions of the effective cross-section are calculated by subtracting the effective charring depth d_{ef} from initial dimensions of the element. The effective charring depth is expressed:

$$d_{ef}=d_{char,0}+k_0\times d_0=\beta_0\times k_0\times d_0$$

where

d_{ef}	is the effective charring depth
$d_{char,0}$	is the one-dimensional charring depth
β_0	is one dimensional charring rate perpendicular to the grain
t	is the time of fire exposure
k_0	$k_0=1,0$ for $t \geq 20$minutes; $k_0=t/20$ for $t < 20$minutes
d_0	is the zero-strength layer: $d_0 =7$mm

According to König [19], the zero-strength layer is formed linearly in time during the first 20 minutes of fire exposure.

4 Specimens of the fire tests

4.1 Modelling of the specimens

In 2014 Fink [1] developed a probabilistic model of glulam beams with the focus on local weak sections, such as knot clusters and finger joints. First, the model was developed based on two strength and stiffness related indicators measured in laboratory, $E_{dyn,F}$ and $tKAR$. $E_{dyn,F}$ is an abbreviation for a modulus of elasticity calculated based on timber boards eigenfrequency and is considered an average value for the entire board. A knot indicator $tKAR$ (total knot area ratio) is defined by Isaksson [26] as follows - ratio between the projected knot area within a length of 150 mm and the cross-section area; overlapping knots are counted only once. Then the model was extended to machine-grading parameters: an estimation of dynamic modulus of elasticity (E_m), and a knot indicator (K_m), measured by the GoldenEye-706 grading device. These indicators are measured automatically during the grading process of a timber board. A third parameter considered in the estimation model is the locations of a finger joints in the lamellas. The application of the numerical model, using machine measured indicators, was validated with 24 GLT beams having well-known local material properties. Again, very good agreement was identified, between the measured and the estimated material properties. The estimation of the load bearing capacity and the bending stiffness are slightly below the measured values. On average, the underestimation is only (~3%) for the load bearing capacity and (~3%) for the bending stiffness. For further details see Fink [1].

4.2 Bending tests in normal conditions

In 2015, Stadelmann [25] performed 4-point bending tests with glulam beams with well-known set-up to provide a basis for the validation of the prior developed numerical model of Fink [1]. In all, 12 glulam beams of strength classes of GL24h and GL36h were tested. The glulam beams were this time bigger than previously tested in the thesis of Fink [3] in order to investigate the well-known size effect when dealing with timber products. Timber boards were machine-graded with GoldenEye-706 grading device. For the fabrication of the finger joints the adhesive PURBONDR HB S109 (1C-Polyurethan adhesive) is used.

For the surface bonding of the lamellas the adhesive Dynea Prefere 4535 (MUF) is used. Beams with the length of 19,0m are planed to dimensions $b \times h = 178 \times 1000mm$ and beams with the length of 11,4m to dimensions $b \times h = 158 \times 600mm$. Beams were loaded until failure. Test results with the respect to strength properties are given in Table 1. For further information and details see Stadelmann [25].

Table 1. Compilation of the test results and estimated properties.

Beam	F_u [kN]	f_m [MPa]	w_{max} [mm]	$E_{m,g}$ [MPa]	$E_{m,g,G}$ [MPa]	$E_{m,l}$ [MPa]
GL24h-11m-1	155,6	30,2	124,7	10700	11221	10801
GL24h-11m-2	178,7	34,7	138,7	11062	11620	11887
GL24h-11m-3	184,2	35,8	155,1	10337	10822	10737
GL24h-11m-4	152,8	29,7	121,5	10483	10983	10933
GL24h-19m-1	273,5	28,0	191,2	10538	11049	-
GL24h-19m-2	278,8	28,6	199,7	10268	10753	-
GL36h-11m-1	218,7	42,4	127,9	14106	15026	14973
GL36h-11m-2	214,3	41,6	125,1	14162	15090	14507
GL36h-11m-3	197,8	38,4	115,6	13928	14824	14913
GL36h-11m-4	166,2	32,3	97,8	14563	15546	15208
GL36h-19m-1	377,9	38,7	242,1	13349	14180	-
GL36h-19m-1	440,4	45,1	244,0	13559	14417	-

Note: F_u - ultimate load at failure, f_m - calculated bending strength, w_{max} - maximum displacement in mid-span, $E_{m,g}$: shear modulus neglected, $E_{m,g,G}$: shear modulus considered (G = 650 MPa), $E_{m,l}$ - local bending stiffness.

4.3   Specimens of the fire test

Six glued laminated timber beams in total with well-known local material properties were tested in fire in the present research. These specimens were cut out of least influenced parts of glued laminated timber beams of originally larger dimensions, previously tested until failure in four point bending tests in normal conditions. The bending tests were performed at ETH Zürich in the master thesis of Stadelmann [25]. Figure 9 shows the original position of the beams in the longer beams already tested.
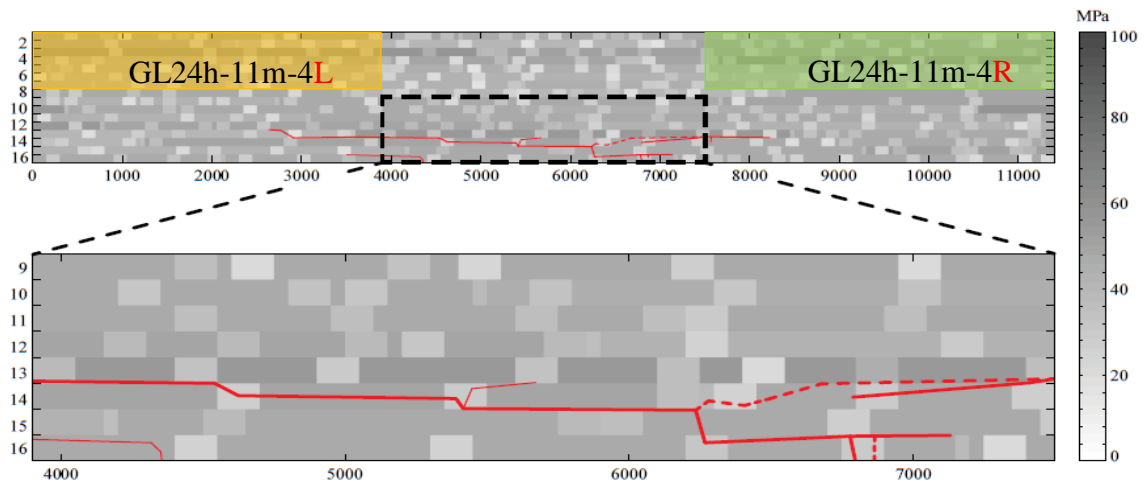
Figure 9. Positions of the fire test specimens in the original beam tested at normal temperature; here example for beam GL24h-11m-4 (Stadelmann, 2015)

After the tests at normal temperature, the specimens tested in fire were cut out and transported to Stockholm.

The beams tested at normal conditions had been labelled accordingly to the strength class of material and specimen length. Original names were substituted with more convenient number markings as shown in Table 2.

Table 2. Overview labelling of fire test specimens

Shortened marking	Original label
1	GL24h – 11m – 4R
2	GL36h – 11m – 2R
3	GL36h – 11m – 4R
4	GL24h – 11m – 4L
5	GL36h – 11m – 3R
6	GL36h – 11m – 4L

Furthermore, each face of every beam was given a face identification letter, „A", „B", „C" or „D", and 200mm step markings were drawn in order to determine the exact positioning in the data processing phase. Detailed photographs of each side of each specimen have also been taken. Pictures to describe the assembly of the specimens can be found in the

appendix A; examples are shown in Figure 10 and Figure 11. Further pictures are saved on the SP server.

Figure 10. Beam face markings on specimens 5 and 6

Figure 11. Local detail of a specimen

After photographing, all specimens were thoroughly inspected for cracks or any other kind of deteriorations which might have an influence on the load bearing capacity and thus also to the fire resistance of the beams. Prior to the fire tests, all beams were weighed, their geometric dimensions and moisture content measured and density calculated. The gathered data is presented in Table 3 and in Table 4.

Table 3. Gathered data of specimens

Specimen	Strength class	Length	Width (mid sect.)	Height (mid sect.)	Weight	Moisture content, avg.	Density
		[mm]	[mm]	[mm]	[kg]	[%]	[kg/m³]
1	GL24h	3889	157	254	67,06	12,6	377,9
2	GL36h	3749	158	256	73,78	12,0	428,2
3	GL36h	3882	158	256	77,68	10,9	440,8
4	GL24h	3889	158	253	65,40	10,9	374,8
5	GL36h	3874	157	253	78,98	10,7	458,3
6	GL36h	3620	157	217	61,38	11,0	442,9

Note: Moisture excluded from calculated density, thus ρ_0 being the dry density is given.

Table 4. Measured lamella heights.

| Specimen		1	2	3	4	5	6
Lamella heights [mm]	1	26	25	25	25,5	24	26
	2	38,5	38,5	39	38,5	38,5	39
	3	38,5	39	38	38	38,5	38
	4	38,5	38,5	39	39	38,5	38,5
	5	38	38,5	38,5	38,5	38	38,5
	6	39,5	38,5	38,5	38,5	38,5	36
	7	34	38	37	35	37	-

Note: Lamella 1 is the top lamella; lamella 7 is the bottom lamella in the fire test

5 Fire tests

5.1 Test program and test parameters.

In the fire tests of three sided exposure the influence of local natural growth imperfections of the structure of wood to load bearing capacity of glued laminated timber beams with well-known local material properties was investigated.

Six specimens of two different strength class with previously surveyed weak sections were loaded and then exposed to standard ISO-fire until failure occurred in a model scale furnace. In the tests with specimen no. 3, 20% of the mean load bearing capacity F_u of bending tests performed at normal temperature was applied. In other five tests the load was 30% of F_u. F_u for each specimen was calculated considering their dimensions. The applied load level throughout the whole test can be taken from Figure 12.
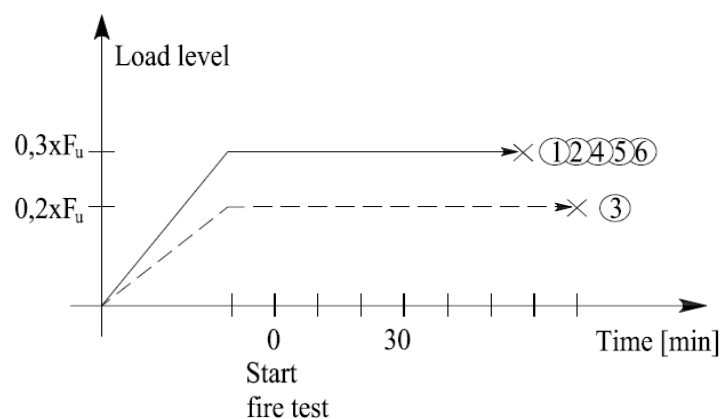
Figure 12. Load level during fire tests with 6 different specimens.

Prior to the tests, all beams were examined and had their physical properties documented (see Section 4.3). Beams were placed onto the furnace with their top faces covered with stone wool in order to protect them from fire. The load was applied up to previously defined level and kept constant. Then, the furnace was switched on and the specimens loaded with constant bending moment until the fire resistance of the beam was reached and failure occurred.

Table 5. Overview of the test program of fire tests.

Specimen name	Strength class	Load level	Load F, [kN]	Parameters tested
1	GL24h	$0,3x\ F_u$	15,8	Time till failure
2	GL36h	$0,3x\ F_u$	20,6	Time till failure
3	GL36h	$0,2x\ F_u$	13,4	Time till failure Temperature inside specimen
4	GL24h	$0,3x\ F_u$	16,0	Time till failure
5	GL36h	$0,3x\ F_u$	20,9	Time till failure
6	GL36h	$0,3x\ F_u$	14,4	Time till failure

Note: Load F is explained in Figure 32.

5.2   Test set-up

Six glued laminated timber beams with well-known local material properties were tested in this research. The properties of these specimens are summarised in Section 3.3. Experiments were conducted in two different sessions: First session in November of 2015 and the second in March 2016. Some changes in the set-up were made after the first session to improve the set-up: load cells replaced, two additional Linear Variable Differential Transformers (LVDT-s) with additional data logger, better preparation process prior to the tests.

All fire tests in this series were performed as "reversed four point bending tests", which means that the load was applied on both ends of the beam and the supports placed in the middle part, see Figure 30 and Figure 31. This reversed set-up still results in a pure bending zone in the mid part of the beam on one hand, but enables the use of a model scale furnace in limited space conditions on the other hand. The load was applied using hydraulic cylinders for pushing beams' ends up, the support details were attached to a furnace's reinforced horizontal edges. The relative displacements were measured using LVDT-s; the comparative absolute displacements were measured by hand at the beam ends using folding ruler. For temperature distribution inside the specimen Type-K wire thermocouples were used.

All the fire tests were performed in the facilities of SP Wood Building Technology, in Drottning Kristinas Väg 67, Stockholm.

5.3 Equipment

5.3.1 Furnace

The used furnace in the SP fire laboratory in Stockholm is custom made by the Danish company J.A. Sandberg. The outer construction is welded together of metal sheets and cold bent stiffening profiles, as shown in Figure 13. The front part of the furnace and five cover details are removable, see Figure 14.
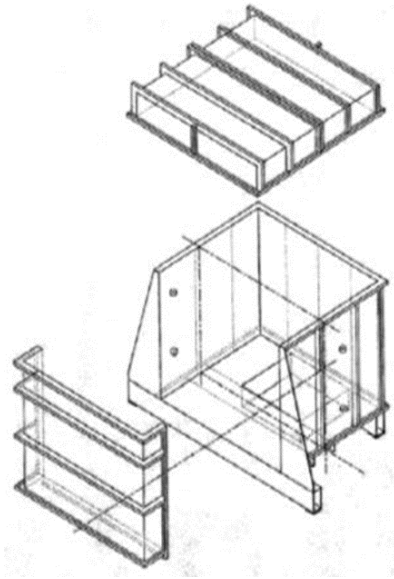
Figure 13.Furnace's steel construction. Image: SP

Figure 14. Furnace's removable front and inner ceramic fibre insulation. Photo: SP

Inside, the metal construction furnace has a 230mm ceramic fibre heat insulation layer, which can be noted in Figure 14. Open inner dimensions are 1000 x 1000 x 1000 [mm], i.e. $1m^3$ of volume. Liquefied petroleum gas is used as fuel, delivered through 4 burners on two different heights on two sides of the furnace. The exhaust gases are mechanically ventilated through an opening in furnace inner floor. The temperature inside the furnace is measured by a pair of plate thermometers, illustrated in Figure 15. The furnace is semi-automatically operated, temperature and pressure inside the furnace must be controlled manually throughout the whole process to follow ISO 834 standard fire curve [20] using a touchscreen interface, see Figure 16.
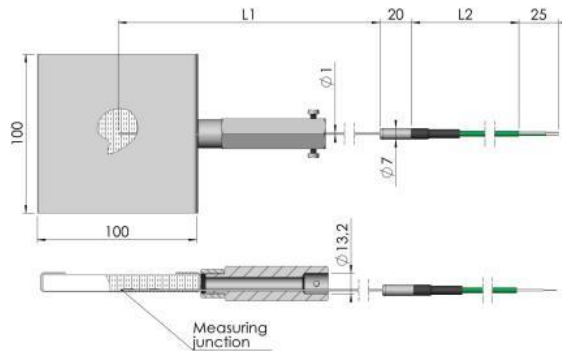
Figure 15. Plate thermocouple in furnace. Image: Pentronic.se

Figure 16. Manual operation of the furnace.

5.3.2 Supports

The supports in these fire tests were custom constructed and made for this project. One support consists of three different details. Two columns are bolted to the furnaces edge using M14 8.8 bolts. The sliding upper detail is quickly removable when not loaded. A standard profile UNP100 and a steel sheet -8mm were used for making the support details. The support in position is presented in Figure 17.

Figure 17. Support details on furnace's

5.3.3 Load application

The load was applied to the glulam beams using a hydraulic system of two cylinders and an electric powered oil pump. The oil pump is manually controlled, but enables easily fine pressure tuning. The length of the cylinders demanded use of additional steel extensioning construction to reach the specimen. The load cell sensors, type AB 50, placed between cylinder's piston rods and extensioners, sent readings to the PC-Logger (see Figure 19) once a second. Load cells were replaced between after the first session of experiments. Please see illustration in. More detailed information is given in Table 6

Figure 18. Hydraulic cylinder with extensioning and load cell sensor in between.

Figure 19. PC-loggers.

5.3.4 Displacement

The set-up change between the first and the second sessions of tests concerns also the deformation measurement. Only one LVDT placed at mid-span was used for measuring relative the displacement in session 1. In session 2, relative and absolute displacements were also measured during the fire tests. Eye readings from a folding carpenter ruler fixed to the hydraulic jack gave absolute displacement values at load application points. These

measurements are not considered to be precise enough to be used for further material properties analysis, but registered for comparative purpose only.

In order to expose the specimens to fire on three sides only the top faces had to be protected. Hard stone wool bats secured with light concrete blocks, 8kg apiece, were fixed on top of the glulam beam using countersunk 6x240mm screws with washers or 8x340mm screws with washers and coil springs. Relative displacements were digitally measured saving readings from LVDT-s with 1 second interval with similar PC-loggers as in Figure 19.

Figure 20. Fixing light concrete blocks on top of the beam.

Figure 21. LVDT transducer used for fire tests. Photo: [27].

Figure 22. Construction for LVDTs during first session.

A specially made wooden construction held the LVTD-s at a suitable height from the blocks. Three LVDT-s were used: One with a measurement range of 100mm in the mid

span, two of 50mm near supports. To take readings from the surface of the beams 8mm steel rods were placed between specimens and the LVDT-s. Short lag screws with cavity on top inside the beams prevented the rods from displacing horizontally. The rods had pointed the lower tip and the cavity in the upper end. As the LVDT-s have coil spring inside, all rods stayed stable during the fire tests. Please see Figure 25. In order to preclude the possibility of receiving false readings because of local crushing of the LVDT holder's legs, their pointed tips were reinforced with aluminium profiles, as shown in Figure 23 and Figure 24.
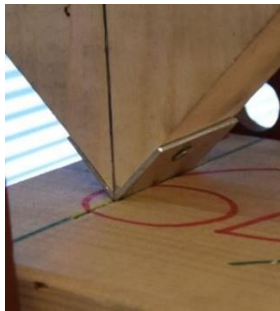
Figure 23. Leg of LVDT construction positioned into a groove.

Figure 24. Metal plate underneath LVDT holder's other leg to ensure smooth slide.

Figure 25. Steel rod between LVDT and lag screw.

5.3.5   Furnace covers

The height of the specimens and the three side exposure to fire demanded using special furnace covers. The steel sheet covers were also custom made. A 1.5mm steel sheet was used for construction. Three layers of soft 50mm stone wool (30 kg/m$^{3)}$, one layer of 50mm

hard stone wool (120 kg/m^3) and one layer of 10mm ceramic fibre insulation were used for inner heat insulation. See Figure 26 and Figure 27.

Figure 26. Placing stone wool insulation on a furnace cover.

Figure 27. Cover ready made.

Notes on the covers during the fire tests:

The covering in a fire test has to be thoroughly considered. The covers used in the current test series were planned to have an extra tightening layer of stone wool between the vertical insulation of covers and the specimen. For the first two experiments the gap was stuffed with torn pieces on soft stone wool left overs. Visually well tightened gaps turned out to be irregular in shapes and unevenly packed, resulting in remarkable smoke in the laboratory. After these two tests insulation of the covers required replacement.

For the third test, tightening wool was properly cut and carefully placed between covers and specimen. Innermost layer of 50mm hard wool and three next layers of 50mm soft wool. This change led to a remarkably diminished leak of smoke. However, an aftermath of forgetting the fact of hard wool not being elastic enough was gaps between the innermost layer of cover insulation and tightening wool, letting fire through to next layers and alongside direction of the sheets. The extent of the fire damage is presented in Figure 28. Obviously,

Figure 28. Result of exposing wool sheets to fire alongside.

31

the insulation of the cover needed to be reassembled again.

For further tests all the tightening bits were cut out of soft stone wool and carefully placed. Please see Figure 33 as an example. Even an extra layer was added in case initially planned four layers did not fully cover and protect the edges of the insulation of the metal covers. Minimum sinking of smoke. Covers could be used for all three remaining fire tests. Must be noted that the covers are not to be used anew without a proper examination.

Altogether insulation of the covers needed to be reassembled twice, after the second test and after the third test.

Most important of obtained experiences can be summarised in following bullet points:

- Prevent exposition of stone wool to fire in any other way than crosswise unless permitted by producer.
- Avoid even fine gaps or cracks in insulation in the side of fire.
- Between the cover and the specimen must be soft deformable insulation.
- Spending extra minutes of time on careful tightening saves hours of insulation reassembling time and material.

5.3.6 Thermocouples

One specimen of the second series, no. 3, had thermocouples placed inside. Type K (chromel-alumel) wire thermocouples were used. The aim was to measure temperature distribution in the middle of the three lowest lamellas in three different locations, illustrated in Figure 29. Three step hand drilling without guidance using 70mm, 153mm and 306mm long 1.5mm drill bits created the channels for the wires. Considering the latter, only trustworthy coordinate is depth, which was easily controllable. Uncertainty of the location of the thermocouples explain received unexpected readings.
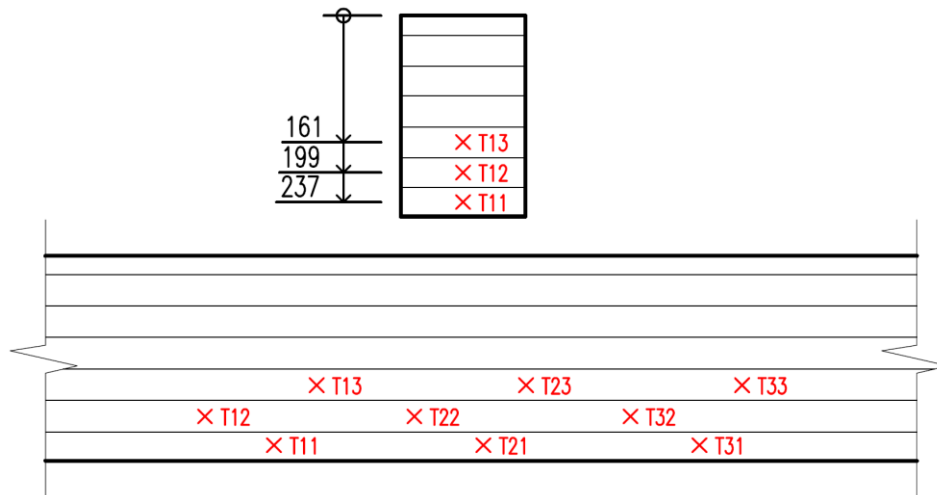
Figure 29. Locations of thermocouples in specimen no. 3.

Table 6. Overview table of used equipment.

Combined horizontal/vertical furnace

Company:	J.A. Sandberg, (Denmark, 2009)
Volume:	1000 mm x 1000 mm x 1000 mm (1 m^3)
Openings:	- max. horizontal opening 1000 mm x 1000 mm - Vertical opening 1000 mm x 1000 mm - Combined opening horizontal and vertical
Combustion equipment unit:	Burners: 4x BIC 65, total 260kW (4 x 65 kW)
	Fuel: Liquefied Petroleum Gas (max. 24 kg/h)
Control system:	Automated/ semi-automated/ manually for temperature and pressure.
	Pressure acc. EN 1363-1: 20Pa (overpressure) at the lower surface of a horizontal test specimen on the top of the

furnace. Custom defined pressure value possible.

Fire curves: Standard fire (ISO 834), HC-curve, custom defined curves up till 1 400 C

Measurements: Furnace: pressure, temperature

Loading device

Oil pump

Company:	OMFB, Italy
Hydraulic jacks:	
Company:	Kladivar, by Poclain Hydraulics
Model:	MD18SC
Cylinders:	2x 63/32-400
Volumetric flow rate	Q=1,5l/m
Max. pressure:	180 bar
	5mm/sec in. pos. direction 7mm/sec in neg. direction

Load cell sensors

Company:	Load Indicator AB, Sweden
Load cell type:	AB50
Nominal capacity:	50kN
Nominal output sensitivity (N.O.):	2,0 +/- 0,1% mV/V
Linearity deviation:	<+/- 0,1% of N.O.
Permissible temperature range:	-30 … +70 Degrees of Celsius
Protection marking:	IP65

LVDT-s

Company:	Micro-Measurements (Division of Vishay Precision Group), NC, USA.

Type:	HS50, ID: (50857946) – [input line 5]
	HS50, ID: (M65331) – [input line 3]
	HS100, ID: (50836863) – [input line 4]
Linear range:	0…50.80mm
Linearity:	±0.35%
Actuator type:	Round shaft
Operating temperature:	-10°C … 60°C

5.3.7 Position of specimens.

During the first session of tests, glulam beams were placed onto the furnace and photographs were taken of their exact location with a ruler in the background. Before the second session of experiments, the positioning had been improved. Prior to the actual fire tests, specimens pervaded a short preparation process. Locations for supports and load application points were marked, top centre line drawn and lag screws for LVDT extension rods inserted. While already in the laboratory, specimens were placed according to prepared markings. Detailed positioning dimensions can be found in Table 7.

Figure 30. Test set-up: specimen positioning, supports, load application, displacement.
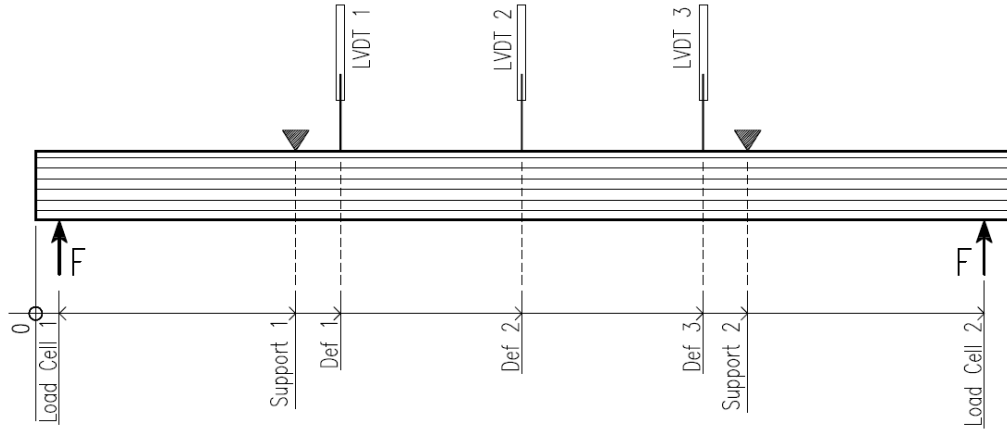
Figure 31. Test set-up: explanatory drawing for Table 7.

Table 7. Test set-up dimensions.

Specimen	Top face	Reference point	Reference point in matrix [mm]	Distance from reference point [mm]							
				Load Cell 1	Support 1	Displacement Def 1	Displacement Def 2	Displacement Def 3	Support 2	Load Cell 2
1	1A	0	3889	85	1083	-	1842	-	2600	3600
2	2C	0	3749	93	1082	-	1845	-	2603	3605
3	3C	0	0	90	1090	1160	1845	2532	2604	3603
4	4C	0	0	90	1090	1160	1850	2540	2610	3610
5	5A	0	3874	75	1075	1140	1835	2530	2595	3595
6	6D	0	0	40	1040	1110	1800	2490	2560	3560
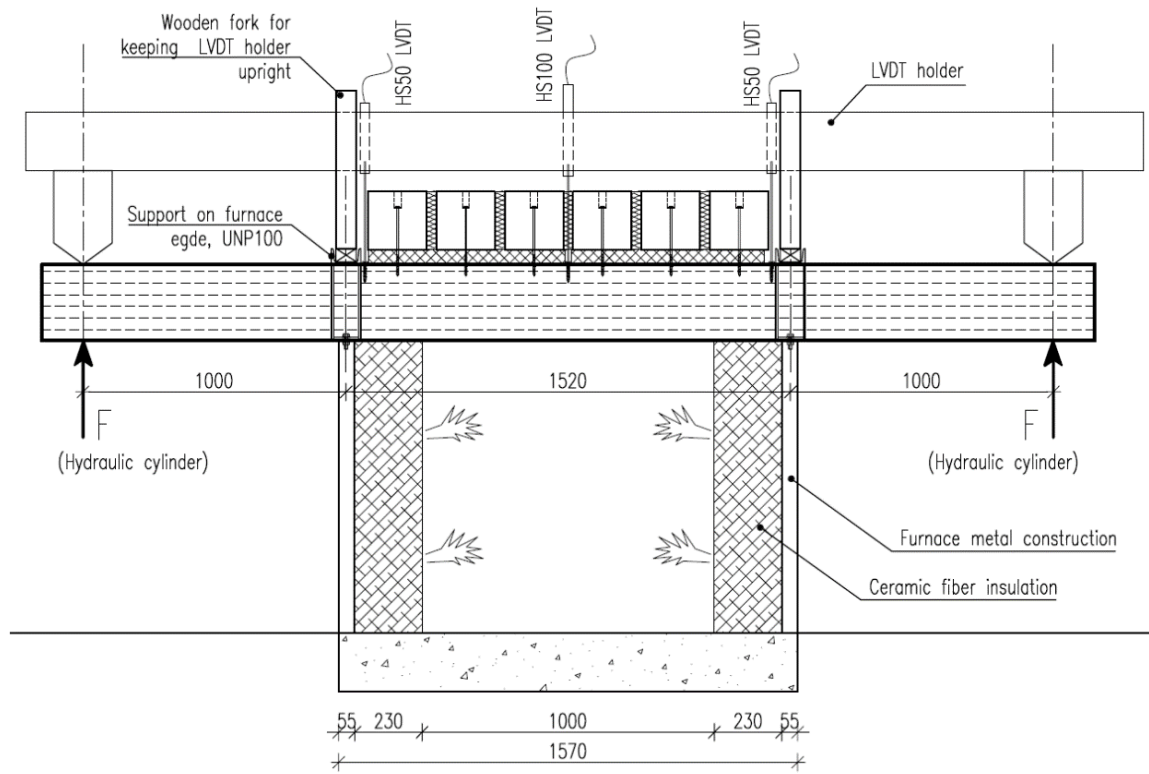
Figure 32. Test set-up: front view, second test session.

Figure 33. Specimen from inside the furnace before ignition the furnace.
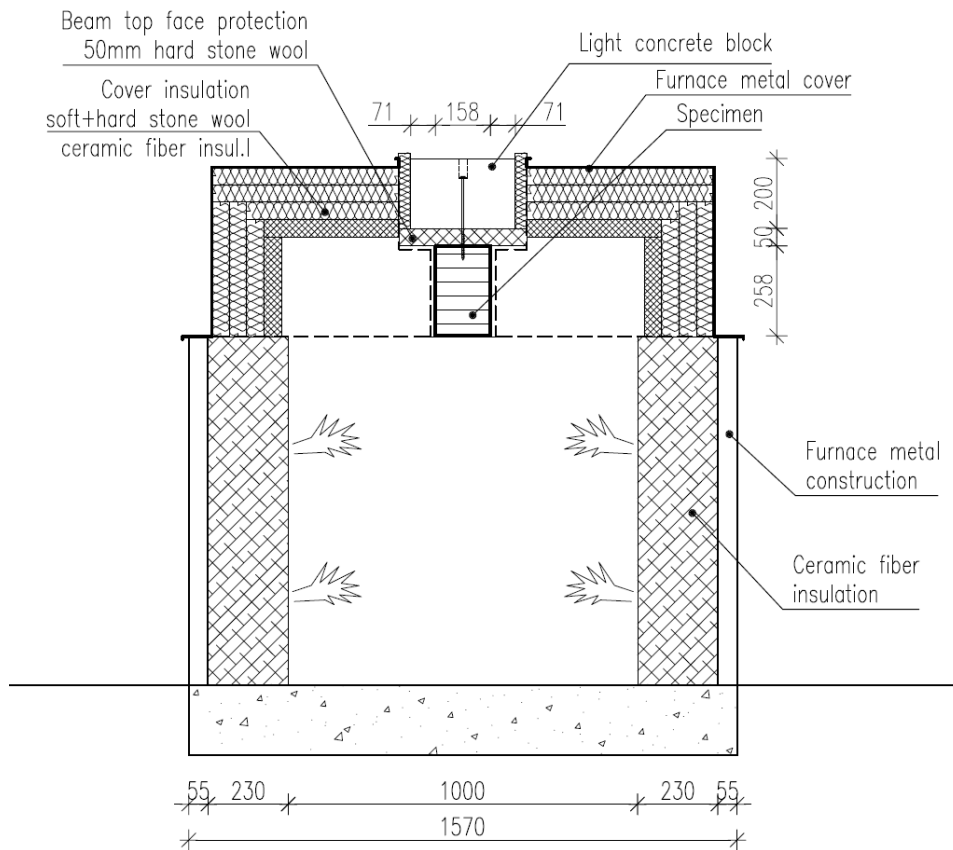
Figure 34. Set-up: section of test set-up.

5.4 Procedure of the test

1) Placing of the specimen

   Placing specimen in accordance to previously prepared markings for supports and load application devices. Locking the supports. Adjusting the location of hydraulic jacks if needed.

2) Placing the covers

   Points "2" and "3" were switched before the second session of tests.

3) Placing the top face protection and tightening materials

   Placing hard stone wool and light concrete blocks on top of the beam, fixing blocks with screws, placing extra tightening soft wool between the beam and the covers near supports, placing tightening wool between the covers and the blocks,

38

photographing beam form inside the furnace (see Figure 33*), close the furnace's front part.*

4) Placing LVDT holder

Placing the wooden frame over the blocks onto the beam, following the exact location of load application line. Placing the LVDT extension rods, ensuring all of them being correctly fixed between LVDT and the lag screw.

5) Applying and keeping the load.

Switch on the oil pump. Take 'zero' readings for hand measurements. Slowly apply the load. Take measurements for different load levels. Monitor load value.

6) Safety protocol

Executing organization's safety protocol points for fire test one by one.

7) Switching on the furnace

Following the process. Burning of the specimens could be observed through a small window. Please see Figure 35.
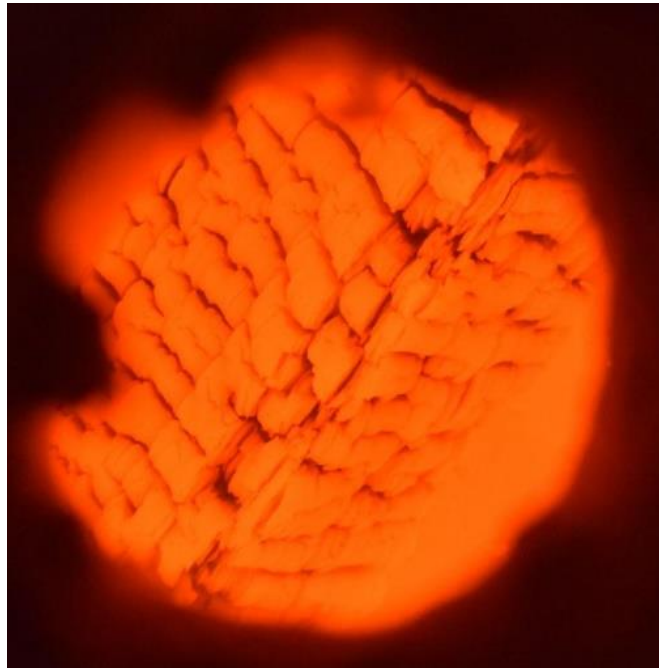
Figure 35. Specimen 3 in fire

8) Taking hand measurement readings

Hand measurements at the load application point were taken with approx. 5 min. interval.

9) Switching off the furnace

   Switching off the furnace, offloading the specimen.

10) Disconnecting and removing measuring devices,

   Right after switching off the furnace disconnect LVDT and thermocouple plugs, remove the LVDT holding frame.

Figure 36. Disconnecting and removing LVDTs.

11) Removing the cover, unlocking supports.

Figure 37. Removing the cover, unlocking the supports.

12) Removing the specimen from furnace

   Removing the specimen from the furnace using chain block, pull it to the more open centre of the room.

Figure 38. Removing specimen

13) Extinguishing the specimen with water

Approximate average time since switching off the furnace until the end of extinguishing the specimen was two minutes. Please see Figure 39. *Let furnace and specimen cool down.*

Figure 39. Extinguishing the specimen

14) Remove the char coal

15) Check the failure type and location

Most beams needed reloading to reveal the location and type of failure. Photographing and/or filming the failure zones.

16) Cutting the specimens.

After the all fire tests specimens were cut in five locations - 140, 160, 180, 200 and 220 cm from reference point – in order to evaluate charring rate.

17) Photographing the cuts.

18) Clean up!

5.5 Test results

Test result have been divided into two subparagraphs of charring and load bearing. Subtracting these aspects serves the interest of clearer information presentation. In addition, for charring analysis all six beams are considered, for load bearing only four tests resulted in trustworthy data due to unexpected problems with the test set-up.

5.5.1 Charring rate

In this research during the second session of experiments information for two different methods of charring depth evaluation was gathered. Photographic multi-lens scanning device enabled saving 3D digital images of actual shape of each specimen after been exposed to fire and charcoal removed. Saved images will be analysed at ETH Zürich later in current year and will not be discussed in detail in this document. In this thesis, a different

Figure 40. Labelling of the cuts. Faces with surface normal pointing towards the end of the beam were marked with letter "A".
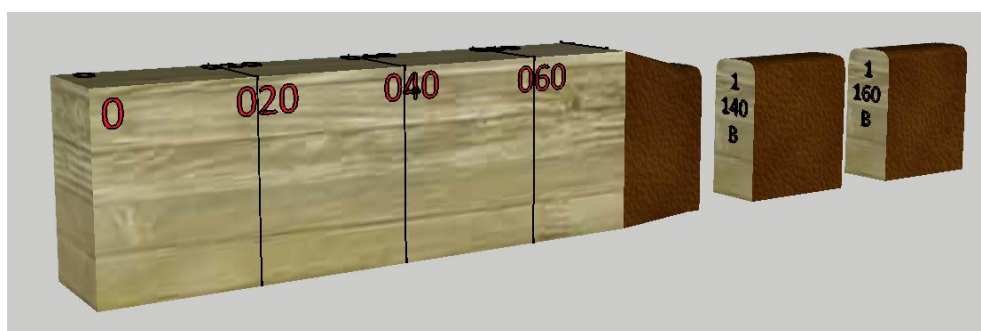

Figure 41. Labelling of the cuts. Faces with surface normal pointing towards the beginning of the beam, local reference system "0", were marked with letter "B".

method is implemented. After scanning, all the beams were cut in the previously defined locations. Five cuts per specimen at locations 140cm, 160cm, 180cm, 200cm and 220cm from beam's reference "0" point. Both faces of each cut were given identification labels, which included beam number, cut location according to reference "0", and an identification letter "A" or "B" depending on the direction face's normal vector; please see illustrations in Figure 40 and Figure 41. All cuts with labels marked on were photographed placed above a ruler using the latter as a scale reference object. Detailed images of the cuts allowed hand drawing cuts' perimeter line with rather high precision in AutoCAD® graphic software. Although each cut has two faces, "A" and "B", only one was chosen for perimeter drawing based on the quality and sharpness of the photograph. As those faces look almost identical but mirrored (see Figure 42) using just one face of the two for charring depth estimation gives totally satisfactory results. Thus, selection of the certain face for presenting a cut is of no importance concerning analysis of notional charring rate in further sections.

In addition, the software has an option of finding the location of area centre and area moment of inertia of the drawn shape of which section moment W of the actual shape of area was calculated:

$$W_y = \frac{I_y}{z_{max}}$$

Both, moment of inertia I_y and distance to the further most point of the section measured from the new centre of gravity z_{max} were obtained from the drawing software. According to Eurocode 5 Part 1-2, in case of three sided exposition to fire, width b and height h of a rectangular section diminish in time in proportion of 2:1 ($b_{notional}$=b-2β_n×t; $h_{notional}$=h-β_n×t). Considering the latter, width, height and section modulus $W_{notional}$ of equivalent notional rectangular cross-section were calculated using an iteration method with a step of 0,01mm.

Average values for each beam are presented in Table 8. More detailed data can be found in the following subsections.

Figure 42. Mirrored shapes of the faces of the same cut. Presented using specimen 4, cut at 200cm from reference starting point "0".

Table 8. Overview of average charring rate and dimensions of notional cross-section.

Beam no.	Original dimensions [mm]		Time in fire [min]	Average notional dimensions [mm]		Mean notional charring rate [mm/min]
	h	b	t	$h_{notional}$	$b_{notional}$	β_n
1	254	157	52:00	213,5	76,0	0,78
2	256	158	49:15	219,4	84,7	0,74
3	256	158	1:08:53	209,0	64,0	0,68
4	253	158	48:06	214,3	80,7	0,80
5	253	157	58:17	211,7	74,5	0,71
6	217	157	44:24	186,1	95,3	0,70
Mean notional charring rate of all specimens:						**0,74**
Coefficient of variation:						**6,57%**

5.5.1.1 Charring of Beam "1"

Compared to all the other beams that were tested until failure, beam "1" was noticeably more deformed as a result of the loaded fire test. Some cross-sections of the cuts contained large cracks, which were graphically corrected in order to create a shape of the section immediately before failure. Thus, sections of beam 1 contain a coefficient of interpretation from author's side. Charring behaviour is summarised in Table 9.
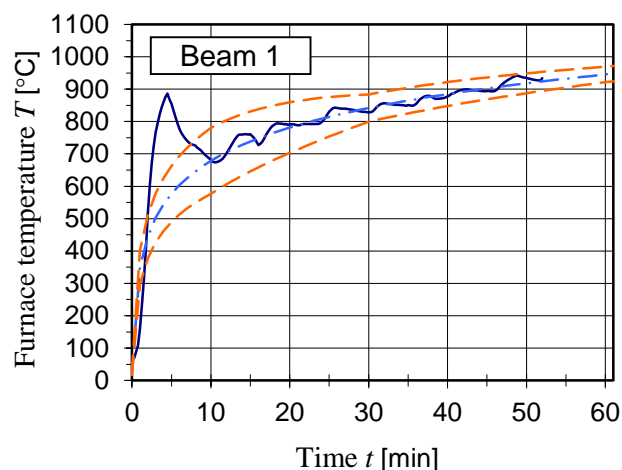
Graph 1. Furnace temperature in fire test on Beam 1 compared to ISO 834 curve and tolerances. Dark blue line represents an average value of two plate thermometers.

As seen in Graph 1, in the beginning of the test temperature inside the furnace exceeded noticeably the ISO 834 [20] curve temperature for 5 minutes by which final results may be influenced.

Table 9. Summary of charring behaviour of the Beam 1

Cut	Initial dimensions		Time in fire	Notional values			Notional charring rate β_n
	h	b	t	h_{not}	b_{not}	W_{not}	
	[mm]	[mm]	[min:sec]	[mm]	[mm]	[mm³]	[mm/min]
140				214,29	77,58	593748,2	0,76
160				213,82	76,64	583983,9	0,77
180	254	157	52:00	212,86	74,72	564252,8	0,79
200				210,69	70,38	520697,9	0,83
220				215,79	80,58	625372,3	0,74
Mean values:				**213,49**	**75,98**		**0,78**
Coefficients of variation:				**0,79%**	**4,45%**		**4,17%**

Cut at 140

Detailed data of the cut 140 of the Beam 1 is given in Table 10 and illustrated in Figure 43.

Table 10. Beam 1 Cut 140

Original section	
h	254mm
b	157mm
W	1688169mm^3
Time in fire	52:00 min
W (actual residual-140)	593781,8 mm^3
Notional section	
h$_{notional}$	214,29 mm
b$_{notional}$	77,58 mm
W$_{notional}$	593748,2 mm^3
Notional charring rate	
β_n	**0,76 mm/min**
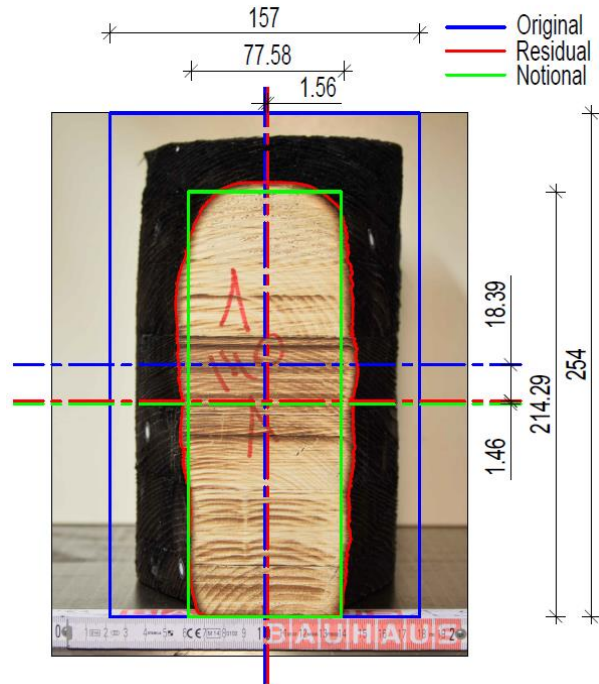
Figure 43. Charring of the Beam 1 cut 140

Cut at 160

Detailed data of the cut 160 of the Beam 1 is given in Table 11 and illustrated in Figure 44.

Table 11. Beam 1 Cut 160

Original section	
h	254 mm
b	157 mm
W	1688169 mm^3
Time in fire	52:00 min
W (actual residual-160)	584105,3 mm^3
Notional section	
h$_{notional}$	213,82 mm
b$_{notional}$	76,64 mm
W$_{notional}$	583983,9 mm^3
Notional charring rate	
β_n	**0,77 mm/min**

Figure 44. Charring of the Beam 1 cut 160
Note: Graphically corrected.
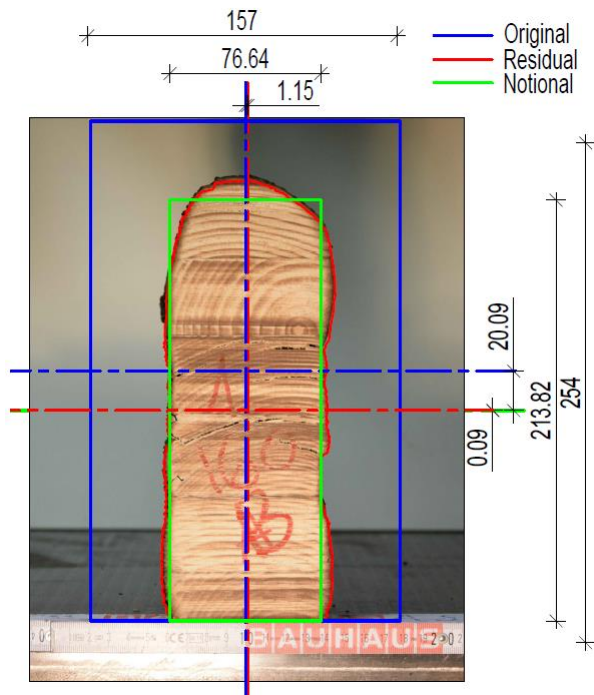
Cut at 180

Detailed data of the cut 180 of the Beam 1 is given in Table 12 and illustrated in Figure 45.

Table 12. Beam 1 Cut 180

Original section	
h	254 mm
b	157 mm
W	1688169 mm^3
Time in fire	52:00 min
W (actual residual-180)	564453,4 mm^3
Notional section	
$h_{notional}$	212,86 mm
$b_{notional}$	74,72 mm
$W_{notional}$	564252,8 mm^3
Notional charring rate	
β_n	**0,79 mm/min**

Figure 45. Charring of the Beam 1 cut 180
Note: Graphically corrected.

Cut at 200

Detailed data of the cut 200 of the Beam 1 is given in Table 13 and illustrated in Figure 46.

Table 13. Beam 1 Cut 200

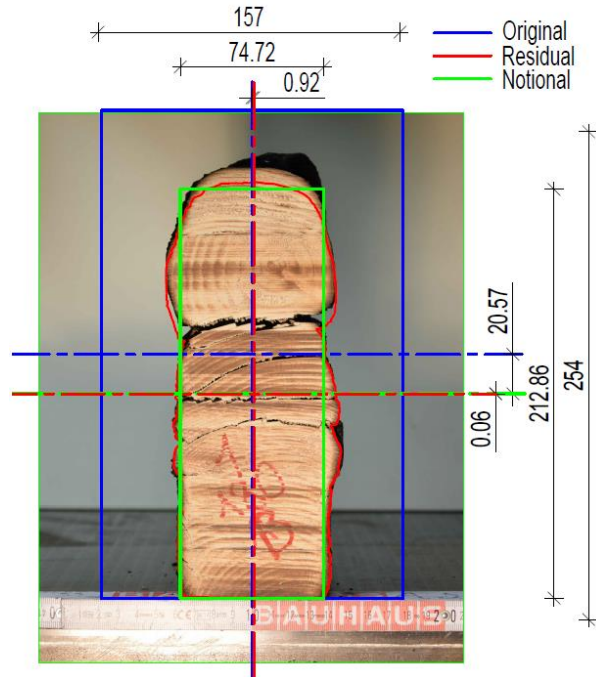| Original section	
h	254 mm
b	157 mm
W	1688169 mm^3
Time in fire	52:00 min
W (actual residual-200)	520879,3 mm^3
Notional section	
$h_{notional}$	210,69 mm
$b_{notional}$	70,38 mm
$W_{notional}$	520697,9 mm^3
Notional charring rate	
β_n	**0,83 mm/min**
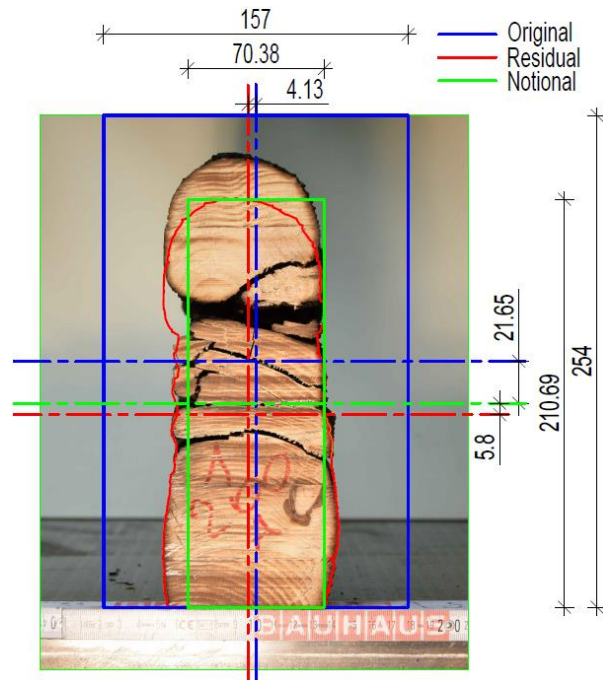
Figure 46. Charring of the Beam 1 cut 200
Note: Graphically corrected.

Cut at 220

Detailed data of the cut the 220 of the Beam 1 is given in Table 14 and illustrated in Figure 47.

Table 14. Beam 1 Cut 220

Original section	
h	254 mm
b	157 mm
W	1688169 mm^3
Time in fire	52:00 min
W (actual residual-220)	625425,8 mm^3
Notional section	
$h_{notional}$	215,79 mm
$b_{notional}$	80,58 mm
$W_{notional}$	625372,3 mm^3
Notional charring rate	
β_n	**0,74 mm/min**

Figure 47. Charring of the Beam 1 cut 220

48

5.5.1.2   Charring of Beam "2"

The average furnace temperature during the fire test of the beam 2 is presented in Graph 2. The summary of the results with respect to charring can be found in Table 15.

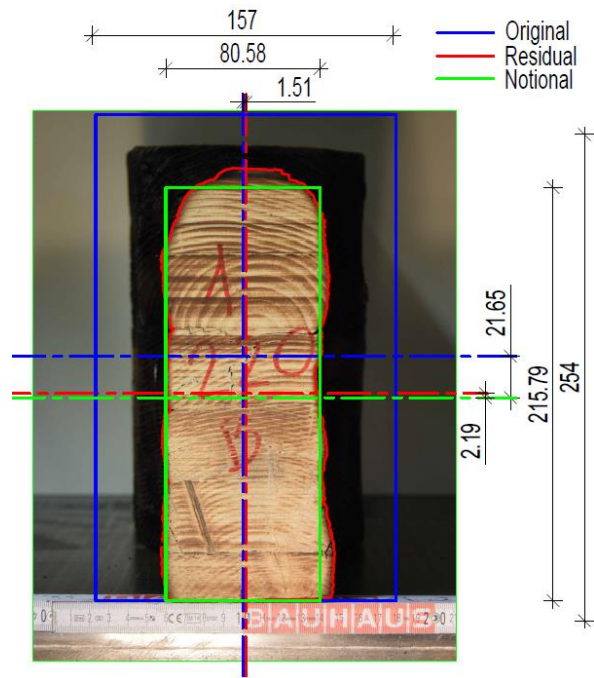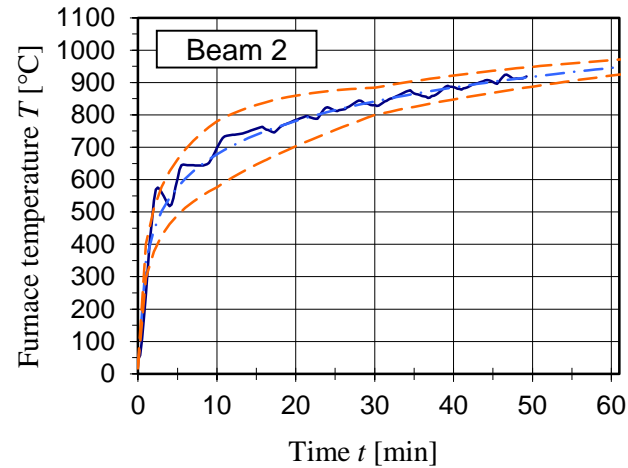*Graph 2. Furnace temperature in fire test on Beam 2 compared to ISO 834 curve and tolerances. Dark blue line represents an average value of two plate thermometers.*

Table 15. Summary of charring behaviour of the Beam 2

Cut	Initial dimensions		Time in fire	Notional values			Notional charring rate β_n
	h	b	t	h_{not}	b_{not}	h	
	[mm]	[mm]	[min:sec]	[mm]	[mm]	[mm]	[mm]
140				218,58	83,16	662287,5	0,76
160				219,46	84,92	681646,6	0,74
180	256	158	49:15	218,80	83,60	667104,1	0,76
200				219,00	84,00	671496,2	0,75
220				221,01	88,02	716574,3	0,71
Mean values:				**219,37**	**84,74**		**0,74**
Coefficients of variation:				**0,40%**	**2,05%**		**2,37%**

Cut at 140

Detailed data of the cut 140 of the Beam 2 is given in Table 16 and illustrated in Figure 48.

Table 16. Beam 2 Cut 140

Original section	
h	256 mm
b	158 mm
W	1725781 mm^3
Time in fire	49:15 min
W (actual residual-140)	662322,5 mm^3
Notional section	
h$_{notional}$	218,58 mm
b$_{notional}$	83,16 mm
W$_{notional}$	662287,5 mm^3
Notional charring rate	
β_n	**0,76 mm/min**

Figure 48. Charring of the Beam 2 cut 140

Cut at 160

Detailed data of the cut 160 of the Beam 2 is given in Table 17 and illustrated in Figure 49.

Table 17. Beam 2 Cut 160

Original section	
h	256 mm
b	158 mm
W	1725781 mm^3
Time in fire	49:15 min
W (actual residual-160)	681739,3 mm^3
Notional section	
h$_{notional}$	219,46 mm
b$_{notional}$	84,92 mm
W$_{notional}$	681646,6 mm^3
Notional charring rate	
β_n	**0,74 mm/min**

Figure 49. Charring of the Beam 2 cut 160

Cut at 180

Detailed data of the cut 180 of the Beam 2 is given in Table 18 and illustrated in Figure 50.

Table 18. Beam 2 Cut 180

Original section	
h	256 mm
b	158 mm
W	1725781 mm^3
Time in fire	49:15 min
W (actual residual-180)	667127,0 mm^3
Notional section	
h$_{notional}$	218,80 mm
b$_{notional}$	83,60 mm
W$_{notional}$	667104,1 mm^3
Notional charring rate	
β_n	**0,76 mm/min**

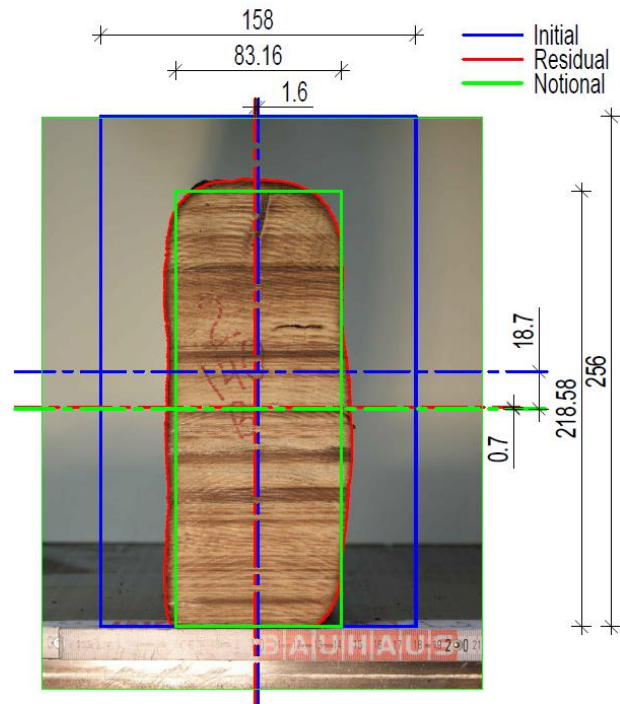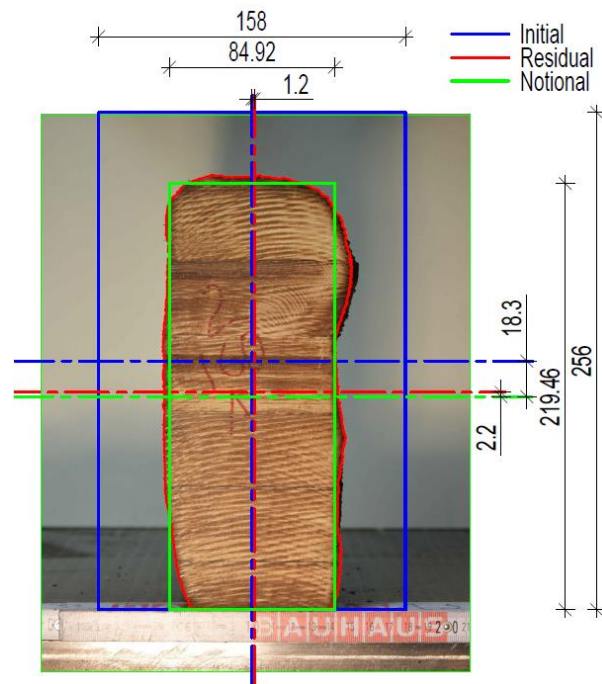*Figure 50. Charring of the Beam 2 cut 180*

Cut at 200

Detailed data of the cut 200 of the Beam 2 is given in Table 19 and illustrated in Figure 51.

Table 19. Beam 2 Cut 200

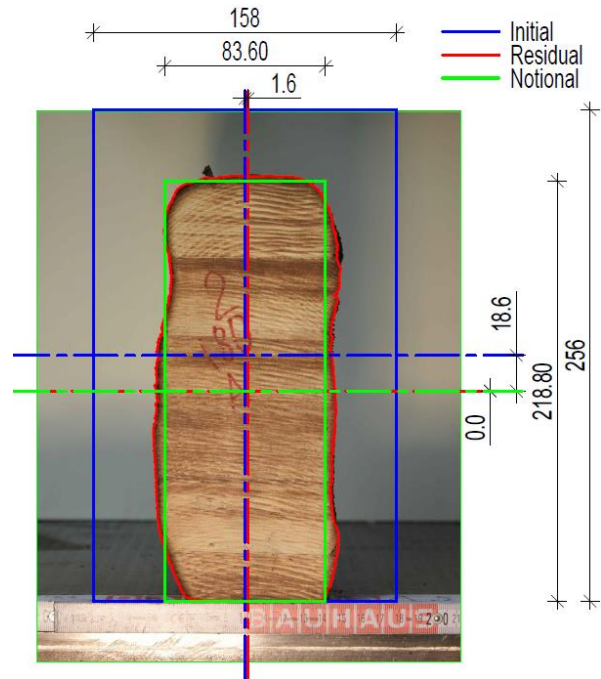| Original section	
h	256 mm
b	158 mm
W	1725781 mm^3
Time in fire	49:15 min
W (actual residual-200)	671571,7 mm^3
Notional section	
h$_{notional}$	219,00 mm
b$_{notional}$	84,00 mm
W$_{notional}$	671496,2 mm^3
Notional charring rate	
β_n	**0,75 mm/min**

Figure 51. Charring of the Beam 2 cut 200

Cut at 220

Detailed data of the cut 220 of the Beam 2 is given in Table 20 and illustrated in Figure 52.

Table 20. Beam 2 Cut 220

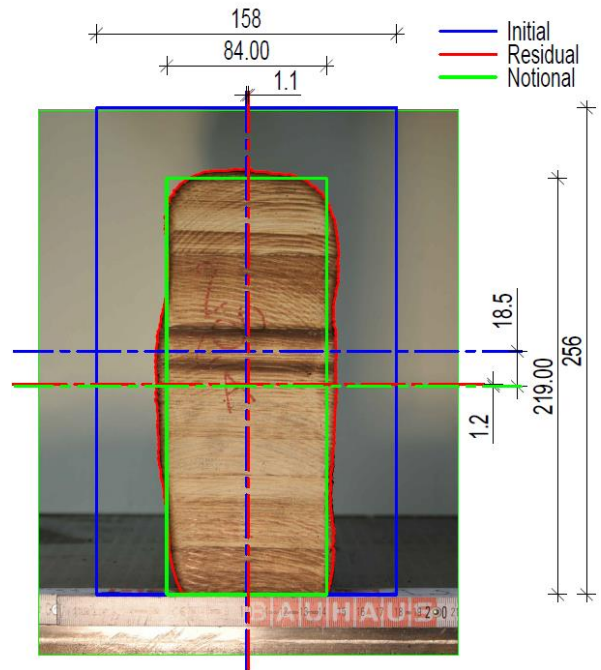| Original section	
h	256 mm
b	158 mm
W	1725781 mm^3
Time in fire	49:15 min
W (actual residual-220)	716617,4 mm^3
Notional section	
h$_{notional}$	221,01 mm
b$_{notional}$	88,02 mm
W$_{notional}$	716574,3 mm^3
Notional charring rate	
β_n	**0,71 mm/min**

Figure 52. Charring of the Beam 2 cut 220

5.5.1.3 Charring of Beam "3"

Different from the other five specimens, beam no. 3 was loaded with a lower load level 0.2 thus, longer resistance in fire and deeper charring could be expected. In addition, beam 3 had nine wire thermocouples drilled into. The positions of the used thermocouples are shown in Figure 29 in Section 5.3.6. The charring behaviour of beam 3 is summarized in Table 21. In Graph 3, the average temperature inside the furnace and in Graph 4 the thermocouple readings inside the specimen are presented.
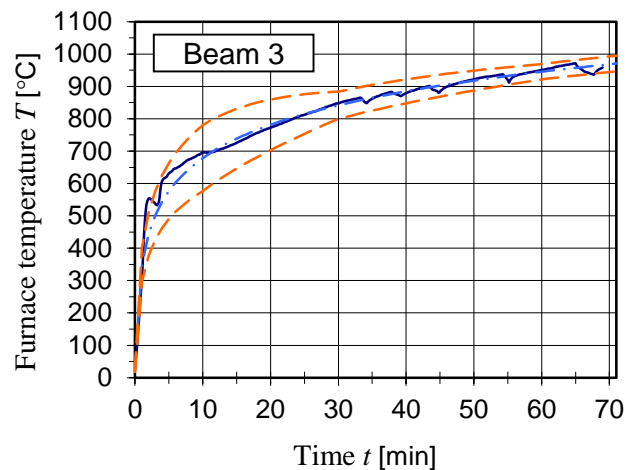
Graph 3. Furnace temperature in fire test on Beam 3 compared to ISO 834 curve and tolerances. Dark blue line represents an average value of two plate thermometers.
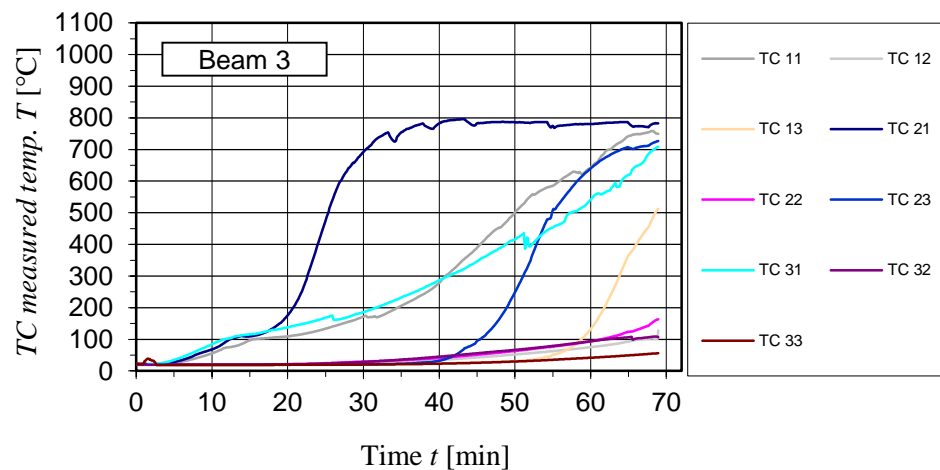
Graph 4. Thermocouple readings inside the Beam 3, position of the thermocouples see Figure 29.

Table 21. Summary of charring behaviour of the Beam 3

Cut	Initial dimensions		Time in fire	Notional values			Notional charring rate β_n
	h	b	t	h_{not}	b_{not}	h	
	[mm]	[mm]	[min:sec]	[mm]	[mm]	[mm]	[mm]
140				209,59	65,18	477204,2	0,67
160				208,38	62,76	454196,5	0,69
180	256	158	68:53	209,29	64,58	471458,8	0,68
200				209,69	65,38	479125,3	0,67
220				208,05	62,10	447997,7	0,70
Mean values:				**209,00**	**64,00**		**0,68**
Coefficients of variation:				**0,32%**	**2,07%**		**1,41%**

Cut at 140

Detailed data of the cut 140 of the Beam 3 is given in Table 22 and illustrated in Figure 53.

Table 22. Beam 3 Cut 140

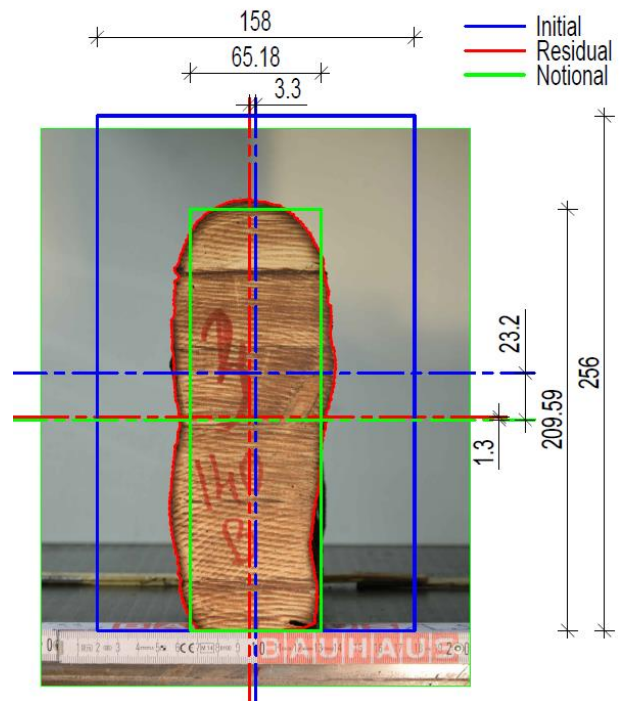| Original section	
h	256 mm
b	158 mm
W	1725781 mm^3
Time in fire	**68:53 min**
W (actual residual-140)	477268,7 mm^3
Notional section	
h$_{notional}$	209,59 mm
b$_{notional}$	65,18 mm
W$_{notional}$	477204,2 mm^3
Notional charring rate	
β_n	**0,67 mm/min**

Figure 53. Charring of the Beam 3 cut 140

Cut at 160

Detailed data of the cut 160 of the Beam 3 is given in Table 23 and illustrated in Figure 54.

Table 23. Beam 3 Cut 160

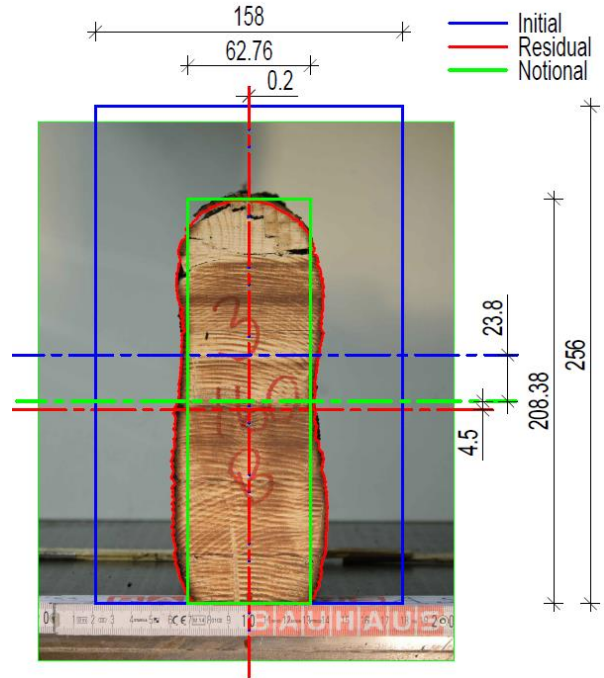| Original section	
h	256 mm
b	158 mm
W	1725781 mm^3
Time in fire	68:53 min
W (actual residual-160)	454257,1 mm^3
Notional section	
h$_{notional}$	208,38 mm
b$_{notional}$	62,76 mm
W$_{notional}$	454196,5 mm^3
Notional charring rate	
β_n	**0,69 mm/min**

Figure 54. Charring of the Beam 3 cut 160
Note: Graphically corrected

Cut at 180

Detailed data of the cut 180 of the Beam 3 is given in Table 24 and illustrated in Figure 55.

Table 24. Beam 3 Cut 180

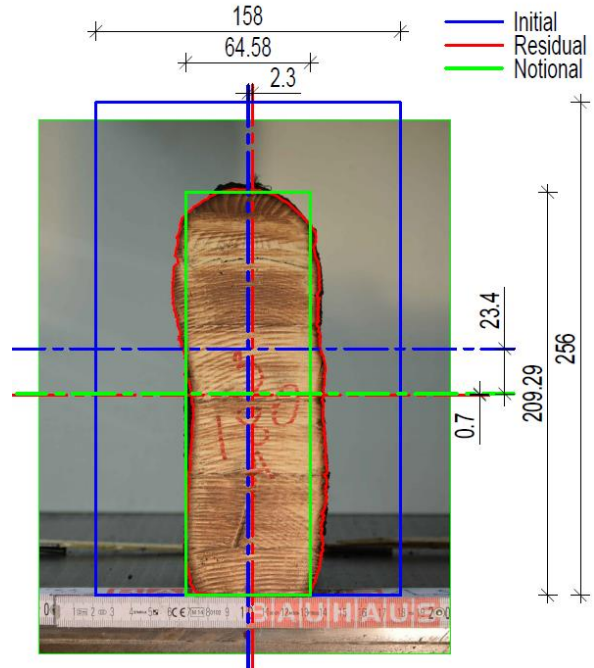| Original section	
h	256 mm
b	158 mm
W	1725781 mm^3
Time in fire	68:53 min
W (actual residual-180)	471539,1 mm^3
Notional section	
h$_{notional}$	209,29 mm
b$_{notional}$	64,58 mm
W$_{notional}$	471458,8 mm^3
Notional charring rate	
β_n	**0,68 mm/min**

Figure 55. Charring of the Beam 3 cut 180.

Cut at 200

Detailed data of the cut 200 of the Beam 3 is given in Table 25 and illustrated in Figure 56.

Table 25. Beam 3 Cut 200

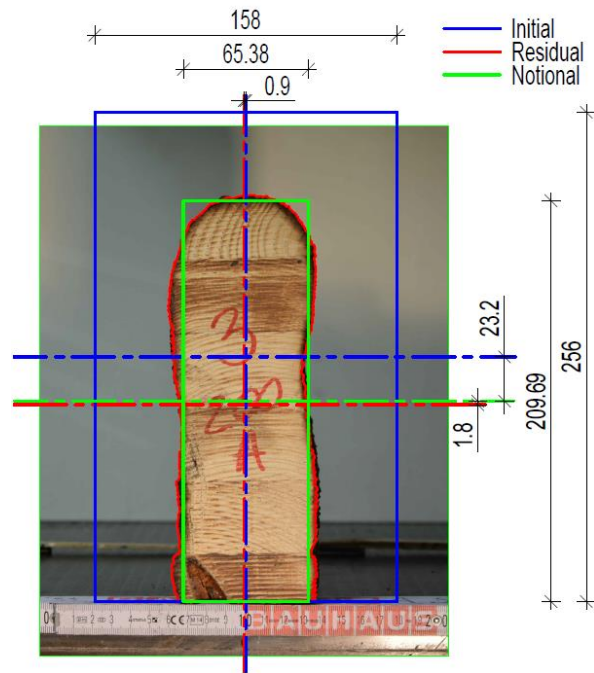| Original section	
h	256 mm
b	158 mm
W	1725781 mm^3
Time in fire	68:53 min
W (actual residual-200)	479150,2 mm^3
Notional section	
h$_{notional}$	209,69 mm
b$_{notional}$	65,38 mm
W$_{notional}$	479125,3 mm^3
Notional charring rate	
β_n	**0,67 mm/min**

Figure 56. Charring of the Beam 3 cut 200

Cut at 220

Detailed data of the cut 220 of the Beam 3 is given in Table 26 and illustrated in Figure 57.

Table 26. Beam 3 Cut 220

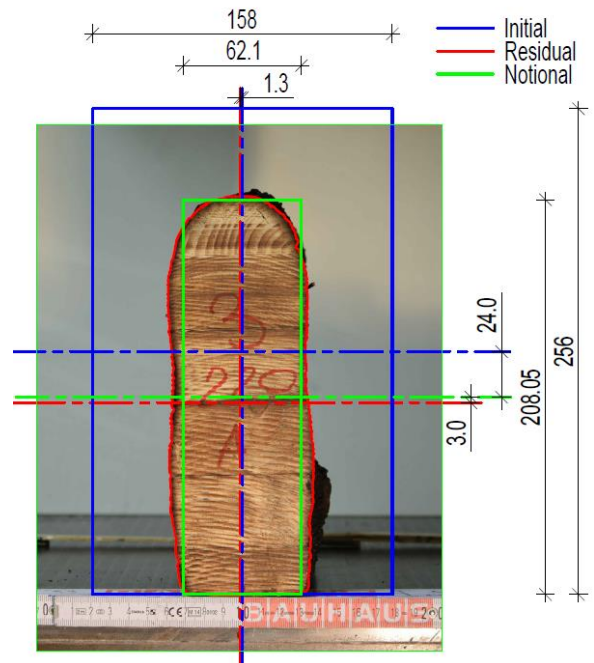| Original section	
h	256 mm
b	158 mm
W	1725781 mm^3
Time in fire	68:53 min
W (actual residual-220)	448081,7 mm^3
Notional section	
h$_{notional}$	208,05 mm
b$_{notional}$	62,10 mm
W$_{notional}$	447997,7 mm^3
Notional charring rate	
β_n	**0,70 mm/min**

Figure 57. Charring of the Beam 3 cut 220

5.5.1.4 Charring of Beam "4"

The charring analyses of the cuts of the beam 4 are summarised in Table 27, the average temperature inside the furnace during the fire test is presented in Graph 5.
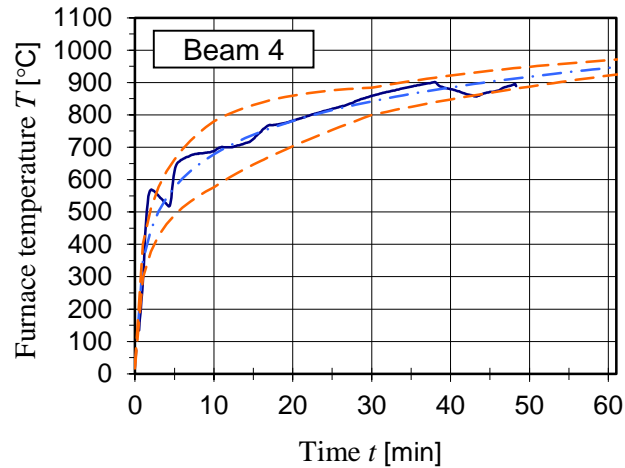
Graph 5. Furnace temperature in fire test on Beam 4 compared to ISO 834 curve and tolerances. Dark blue line represents an average value of two plate thermometers.

Table 27. Summary of charring behaviour of the Beam 4

Cut	Initial dimensions		Time in fire	Notional values			Notional charring rate β_n
	h	b	t	h_{not}	b_{not}	h	
	[mm]	[mm]	[min:sec]	[mm]	[mm]	[mm]	[mm]
140				213,52	79,04	600582,7	0,82
160				215,90	83,80	651025,6	0,77
180	253	158	48:06	213,55	79,10	601207,5	0,82
200				214,54	81,08	621983,8	0,80
220				214,17	80,34	614183,1	0,81
Mean values:				**214,34**	**80,67**		**0,80**
Coefficients of variation:				**0,41%**	**2,16%**		**2,25%**

57

Cut at 140

Detailed data of the cut 140 of the Beam 4 is given in Table 28 and illustrated in Figure 58.

Table 28. Beam 4 Cut 140

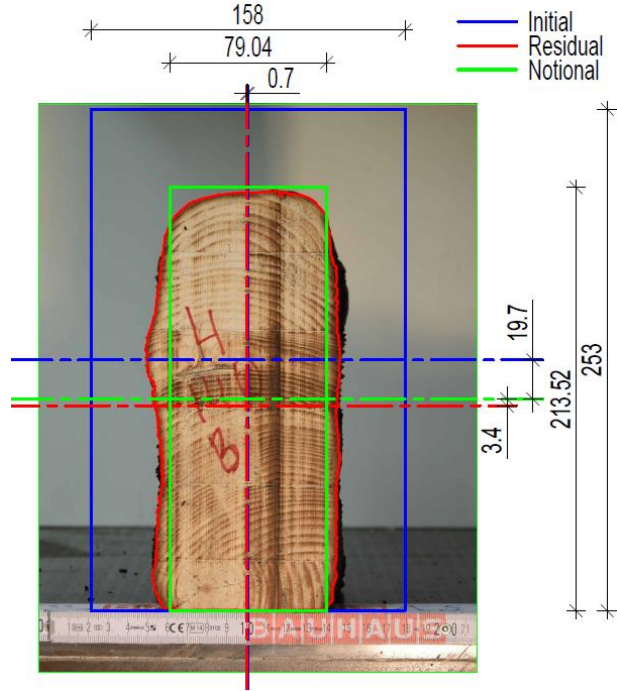| Original section	
h	253 mm
b	158 mm
W	1685570 mm^3
Time in fire	48:06 min
W (actual residual-140)	600649,9 mm^3
Notional section	
h$_{notional}$	213,52 mm
b$_{notional}$	79,04 mm
W$_{notional}$	600582,7 mm^3
Notional charring rate	
β_n	**0,82 mm/min**

Figure 58. Charring of the Beam 4 cut 140

Cut at 160

Detailed data of the cut 160 of the Beam 4 is given in Table 29 and illustrated in Figure 59.

Table 29. Beam 4 Cut 160

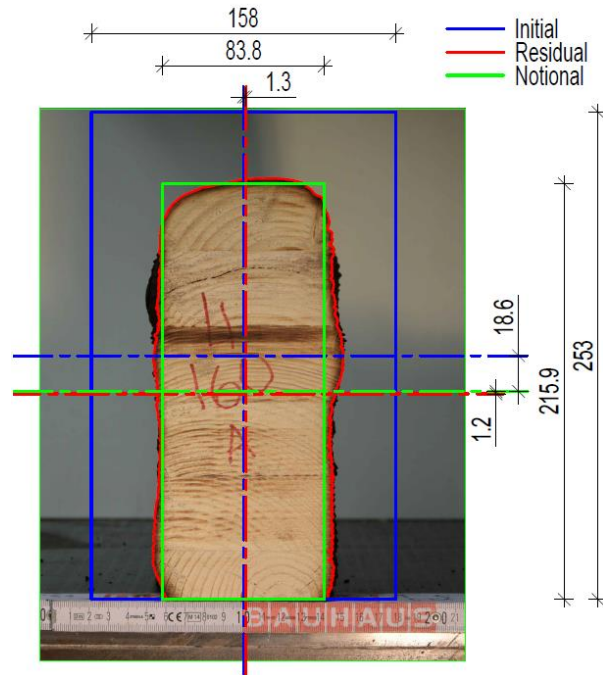| Original section	
h	253 mm
b	158 mm
W	1685570 mm^3
Time in fire	48:06 min
W (actual residual-160)	651169,1 mm^3
Notional section	
h$_{notional}$	215,90 mm
b$_{notional}$	83,80 mm
W$_{notional}$	651025,6 mm^3
Notional charring rate	
β_n	**0,77 mm/min**

Figure 59. Charring of the Beam 4 cut 160

Cut at 180

Detailed data of the cut 180 of the Beam 4 is given in Table 30 and illustrated in Figure 60.

Table 30. Beam 4 Cut 180

Original section	
h	253 mm
b	158 mm
W	1685570 mm^3
Time in fire	48:06 min
W (actual residual-180)	601393,8 mm^3
Notional section	
h$_{notional}$	213,55 mm
b$_{notional}$	79,10 mm
W$_{notional}$	601207,5 mm^3
Notional charring rate	
β_n	**0,82 mm/min**

Figure 60. Charring of the Beam 4 cut 180.

Cut at 200

Detailed data of the cut 200 of the Beam 4 is given in Table 31 and illustrated in Figure 61.

Table 31. Beam 4 Cut 200

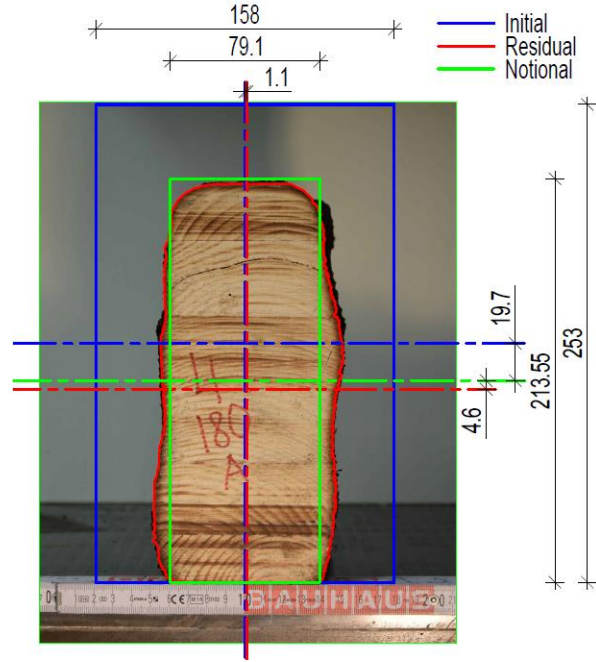| Original section	
h	253 mm
b	158 mm
W	1685570 mm^3
Time in fire	48:06 min
W (actual residual-200)	622128,9 mm^3
Notional section	
h$_{notional}$	214,54 mm
b$_{notional}$	81,08 mm
W$_{notional}$	621983,8 mm^3
Notional charring rate	
β_n	**0,80 mm/min**
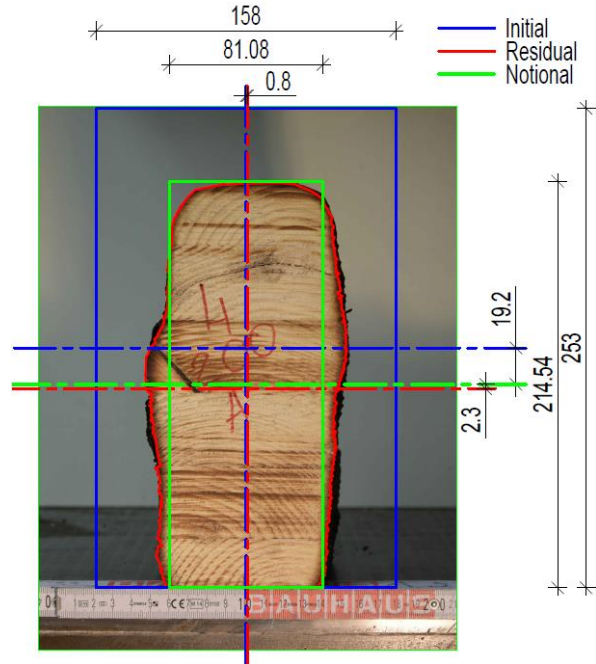
Figure 61. Charring of the Beam 4 cut 200

Cut at 220

Detailed data of the cut 220 of the Beam 4 is given in Table 32 and illustrated in Figure 62.

Table 32. Beam 4 Cut 220

Original section	
h	253 mm
b	158 mm
W	1685570 mm^3
Time in fire	48:06 min
W (actual residual-220)	614230,0 mm^3
Notional section	
h$_{notional}$	214,17 mm
b$_{notional}$	80,34 mm
W$_{notional}$	614183,1 mm^3
Notional charring rate	
β_n	**0,81 mm/min**
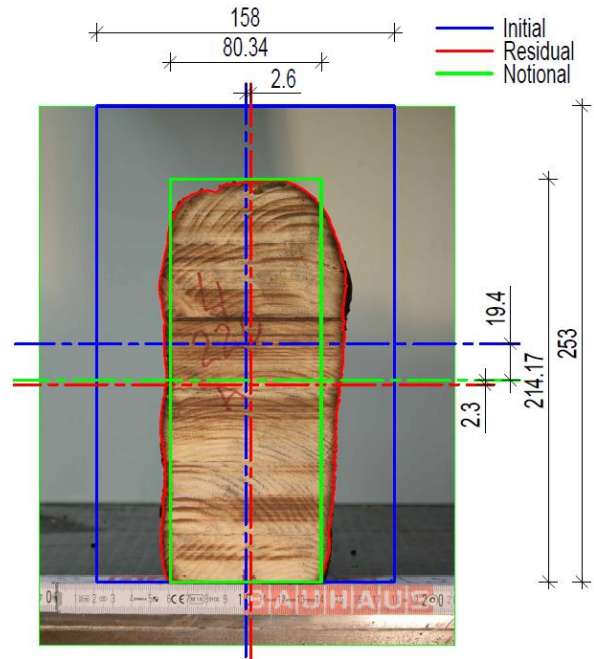
Figure 62. Charring of the Beam 4 cut 220

5.5.1.5 Charring of Beam "5"

The charring analyses of the cuts of the beam 5 are summarised in Table 33. The average temperature inside the furnace during fire test is presented in Graph 6.

Graph 6. Furnace temperature in fire test on Beam 5 compared to ISO 834 curve and tolerances. Dark blue line represents an average value of two plate thermometers.

Table 33. Summary of charring behaviour of the Beam 5

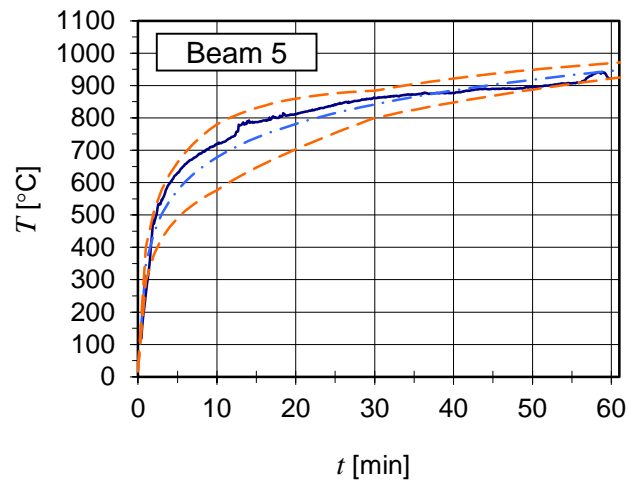| Cut	Initial dimensions		Time in fire t	Notional values			Notional charring rate β_n
	h [mm]	b [mm]	[min:sec]	h_{not} [mm]	b_{not} [mm]	h [mm]	[mm]
140				212,21	75,42	566065,9	0,70
160				212,77	76,54	577508,0	0,69
180	253	157	58:17	211,22	73,44	546074,0	0,72
200				210,72	72,44	536091,2	0,73
220				211,74	74,48	556538,2	0,71
Mean values:				**211,73**	**74,46**		**0,71**
Coefficients of variation:				**0,34%**	**1,93%**		**1,74%**

61

Cut at 140

Detailed data of the cut 140 of the Beam 5 is given in Table 34 and illustrated in Figure 63.

Table 34. Beam 5 Cut 140

Original section	
h	253 mm
b	157 mm
W	1674902 mm³
Time in fire	58:17 min
W (actual residual-140)	566195,9 mm³
Notional section	
$h_{notional}$	212,21 mm
$b_{notional}$	75,42 mm
$W_{notional}$	566065,9 mm³
Notional charring rate	
β_n	**0,70 mm/min**

Figure 63. Charring of the Beam 5 cut 140

Cut at 160

Detailed data of the cut 160 of the Beam 5 is given in Table 35 and illustrated in Figure 64.

Table 35. Beam 5 Cut 160

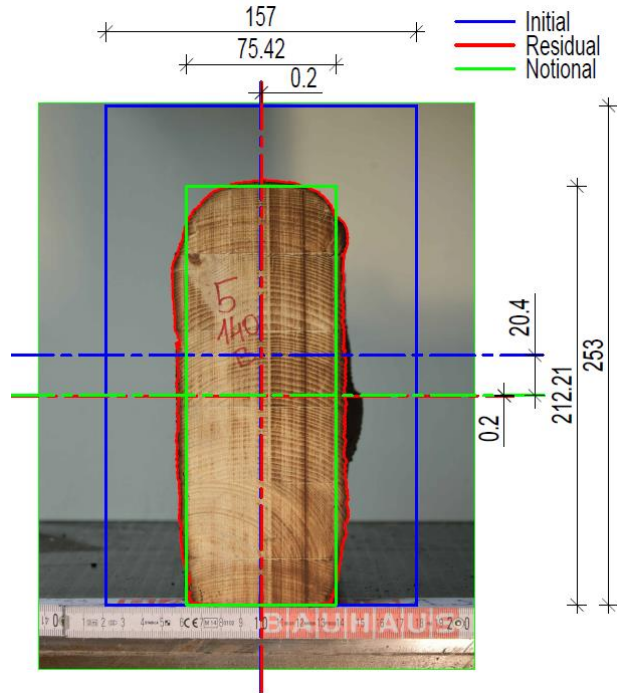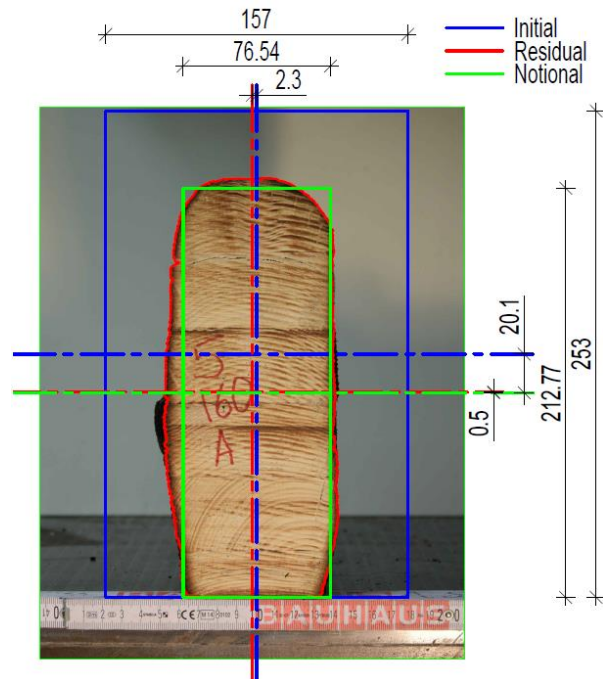| Original section	
h	253 mm
b	157 mm
W	1674902 mm³
Time in fire	58:17 min
W (actual residual-160)	577618,3 mm³
Notional section	
$h_{notional}$	212,77 mm
$b_{notional}$	76,54 mm
$W_{notional}$	577508,0 mm³
Notional charring rate	
β_n	**0,69 mm/min**

Figure 64. Charring of the Beam 5 cut 160

Cut at 180

Detailed data of the cut 180 of the Beam 5 is given in Table 36 and illustrated in Figure 65.

Table 36. Beam 5 Cut 180

Original section	
h	253 mm
b	157 mm
W	1674902 mm^3
Time in fire	58:17 min
W (actual residual-180)	546174,5 mm^3
Notional section	
$h_{notional}$	211,22 mm
$b_{notional}$	73,44 mm
$W_{notional}$	546074,0 mm^3
Notional charring rate	
β_n	**0,72 mm/min**

Figure 65. Charring of the Beam 5 cut 180.

Cut at 200

Detailed data of the cut 200 of the Beam 5 is given in Table 37 and illustrated in Figure 66.

Table 37. Beam 5 Cut 200

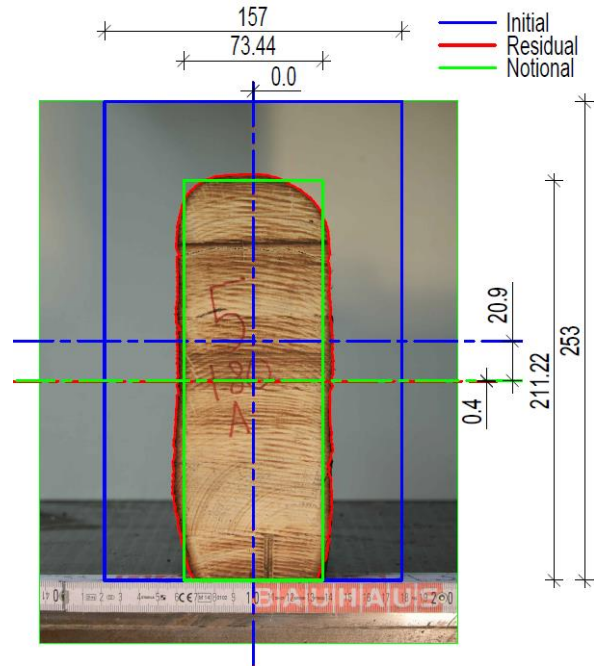| Original section	
h	253 mm
b	157 mm
W	1674902 mm^3
Time in fire	58:17 min
W (actual residual-200)	536156,3 mm^3
Notional section	
$h_{notional}$	210,72 mm
$b_{notional}$	72,44 mm
$W_{notional}$	536091,2 mm^3
Notional charring rate	
β_n	**0,73 mm/min**
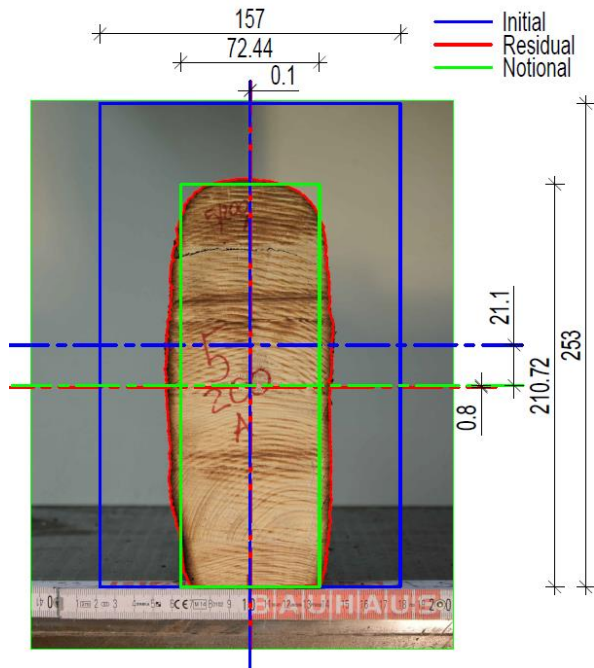
Figure 66. Charring of the Beam 5 cut 200

Cut at 220

Detailed data of the cut 220 of the Beam 5 is given in Table 38 and illustrated in Figure 67.

Table 38. Beam 5 Cut 220

Original section	
h	253 mm
b	157 mm
W	1674902 mm^3
Time in fire	58:17 min
W (actual residual-220)	556570,9 mm^3
Notional section	
h$_{notional}$	211,74 mm
b$_{notional}$	74,48 mm
W$_{notional}$	556537,2 mm^3
Notional charring rate	
β_n	**0,71 mm/min**
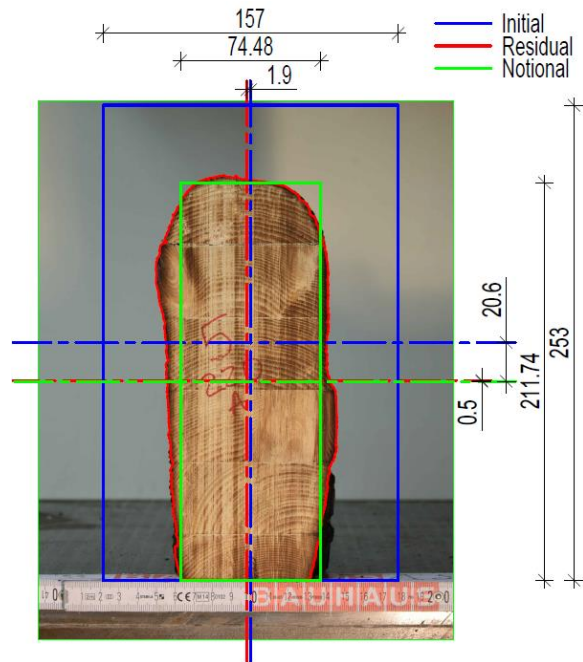
Figure 67. Charring of the Beam 5 cut 220

5.5.1.6 Charring of Beam "6"

The charring behaviour of beam 6 is summarized in Table 39. In Graph 7, the average temperature inside furnace is presented. Unlike with other specimens, first cut of beam 6 was made at 134,6 cm from reference zero "0". The purpose for the alternative location was to maintain the failure section as a whole for further study of the failed finger joint.
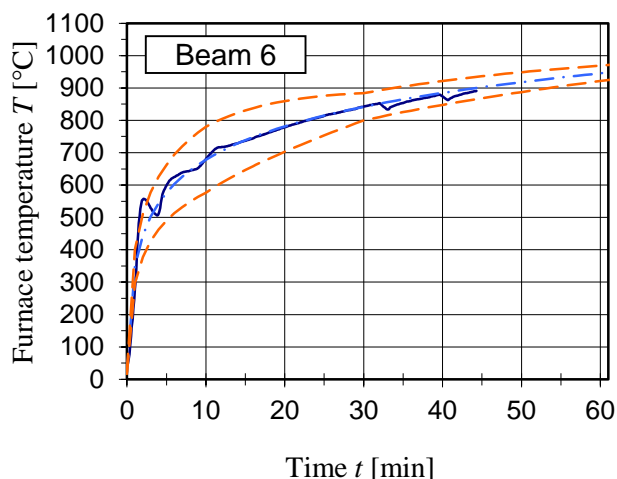
Graph 7. Furnace temperature in fire test on Beam 6 compared to ISO 834 curve and tolerances. Dark blue line represents an average value of two plate thermometers.

Table 39. Summary of charring behaviour of the Beam 6

Cut	Initial dimensions		Time in fire t	Notional values			Notional charring rate β_n
	h	b		h_{not}	b_{not}	h	
	[mm]	[mm]	[min:sec]	[mm]	[mm]	[mm]	[mm]
140				187,42	97,84	572792,2	0,67
160				185,91	94,82	546203,2	0,70
180	217	157	44:24	185,29	93,58	535470,8	0,71
200				186,04	95,08	548467,1	0,70
220				185,97	94,94	547247,5	0,70
Mean values:				**186,13**	**95,25**		**0,70**
Coefficients of variation:				**0,38%**	**1,47%**		**2,27%**

**Cut at 134,6**

Detailed data of the cut 134,6 of the Beam 6 is given in Table 40 and illustrated in Figure 68.

Table 40. Beam 6 Cut 134,6

Original section	
h	217 mm
b	157 mm
W	1232162 mm^3
Time in fire	44:24 min
W (actual residual-140)	572948,6 mm^3
Notional section	
h$_{notional}$	187,42 mm
b$_{notional}$	97,84 mm
W$_{notional}$	572792,2 mm^3
Notional charring rate	
β_n	**0,67 mm/min**

Figure 68. Charring of the Beam 6 cut 134,6

Cut at 160

Detailed data of the cut 160 of the Beam 6 is given in Table 41 and illustrated in Figure 69.

Table 41. Beam 6 Cut 160

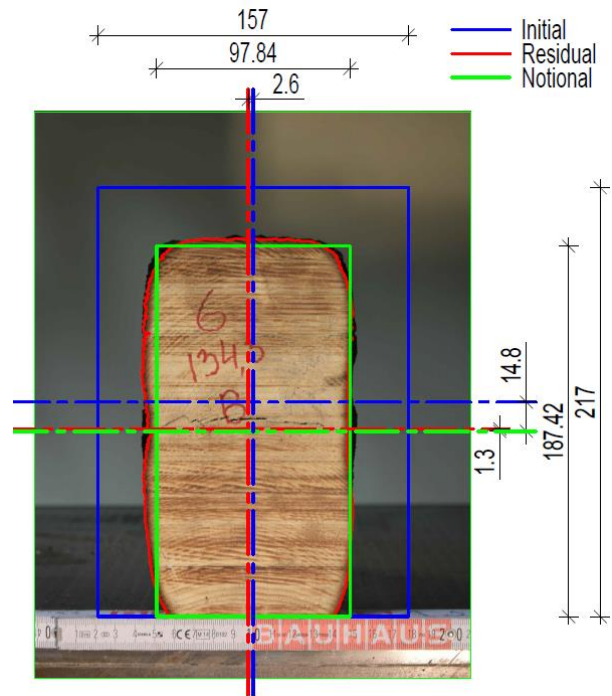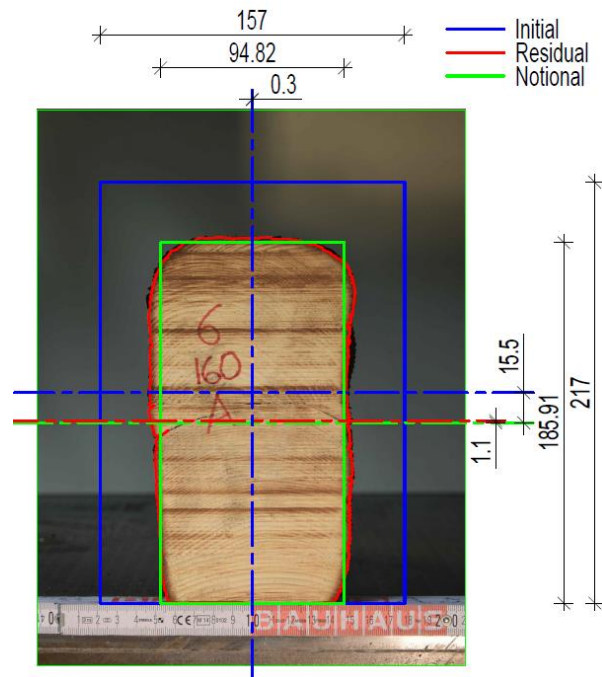| Original section	
h	217 mm
b	157 mm
W	1232162 mm^3
Time in fire	44:24 min
W (actual residual-160)	546374,1 mm^3
Notional section	
h$_{notional}$	185,91 mm
b$_{notional}$	94,82 mm
W$_{notional}$	546203,2 mm^3
Notional charring rate	
β_n	**0,70 mm/min**

Figure 69. Charring of the Beam 6 cut 160

66

Cut at 180

Detailed data of the cut 180 of the Beam 6 is given in Table 42 and illustrated in Figure 70.

Table 42. Beam 6 Cut 180

Original section	
h	217 mm
b	157 mm
W	1232162 mm^3
Time in fire	44:24 min
W (actual residual-180)	535522,7 mm^3
Notional section	
h$_{notional}$	185,29 mm
b$_{notional}$	93,58 mm
W$_{notional}$	535470,8 mm^3
Notional charring rate	
β_n	**0,71 mm/min**

Figure 70. Charring of the Beam 6 cut 180.

Cut at 200

Detailed data of the cut 200 of the Beam 6 is given in Table 43 and illustrated in Figure 71.

Table 43. Beam 6 Cut 200

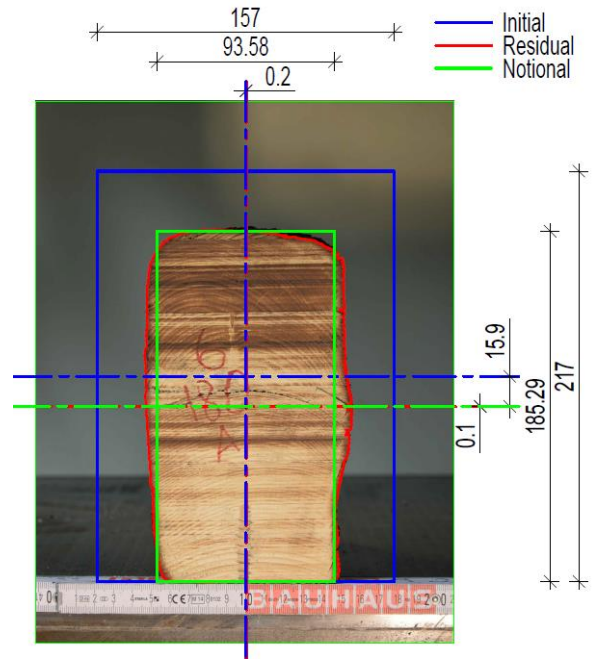| Original section	
h	217 mm
b	157 mm
W	1232162 mm^3
Time in fire	44:24 min
W (actual residual-200)	548542,4 mm^3
Notional section	
h$_{notional}$	186,04 mm
b$_{notional}$	95,08 mm
W$_{notional}$	548467,1 mm^3
Notional charring rate	
β_n	**0,70 mm/min**
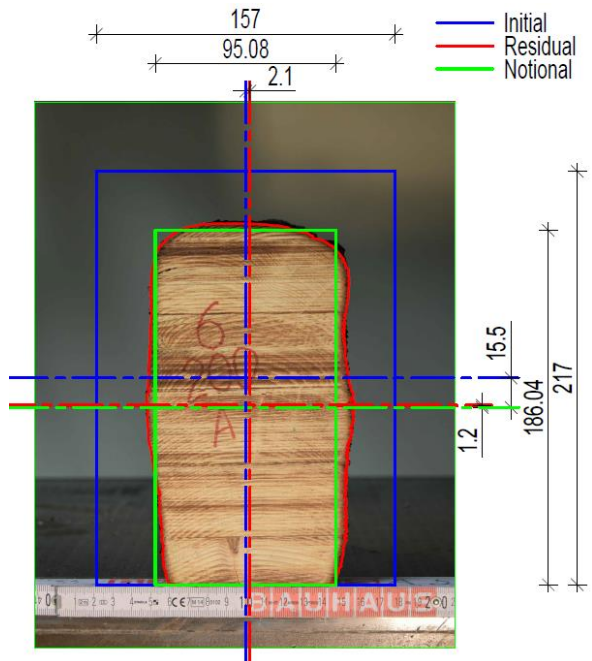
Figure 71. Charring of the Beam 6 cut 200

Cut at 220

Detailed data of the cut 220 of the Beam 6 is given in Table 44 and illustrated in Figure 72.

Table 44. Beam 6 Cut 220

Original section	
h	217 mm
b	157 mm
W	1232162 mm^3
Time in fire	44:24 min
W (actual residual-220)	547323,3 mm^3
Notional section	
h$_{notional}$	185,97 mm
b$_{notional}$	94,94 mm
W$_{notional}$	547247,5 mm^3
Notional charring rate	
β_n	**0,70 mm/min**

Figure 72. Charring of the Beam 6 cut 220

68

5.5.2   Load bearing capacity

In the current section, failure locations and failure types are presented together with calculations of the bending strength of the material in fire and the int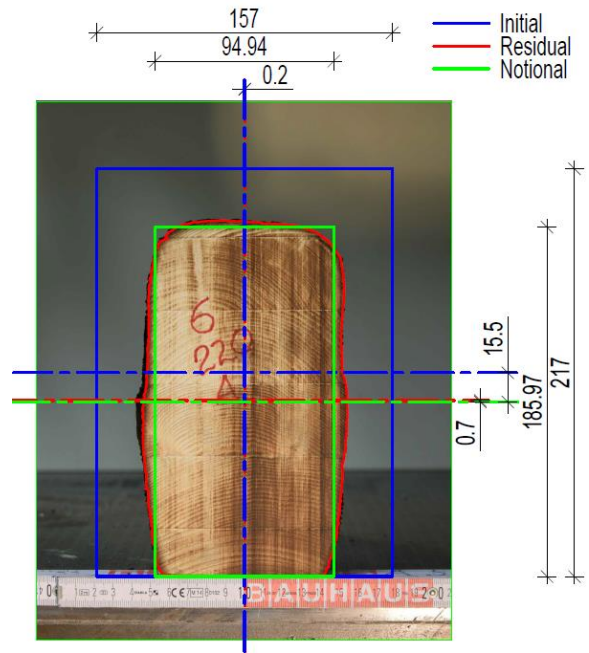erpretation of the zero strength layer d_0. The change of the modulus of elasticity due to the fire exposure will not be discussed within this thesis, but will be analysed in a next step. An overview of the glulam beams' performance in the fire tests is given in Table 45. The fire test results for each specimen will be presented in more detail in the following subsections.

Beams that were tested in the first session, labelled "1" and "2", are excluded from the evaluation of mechanical properties due to the occurred technical complications. While testing specimen "2", loading device failed at 50-th minute, the beam was not broken. Further, load values for experiments with specimens "1" and "2" are not of sufficient certainty.

The load level for the fire tests was chosen 0,2 for Beam 3 and 0,3 for other specimens of the ultimate bending moment in normal conditions. As strength of a timber element can be tested only once in fire, a reference value for normal temperature bending strength had to be determined. The ultimate bending moment for normal conditions was derived from the expected value i.e. a mean value of bending strength in the test series of Stadelmann [25]; see Section 4.2. The load value for each specimen was calculated considering the dimensions and strength class.

The stress at failure (when the fire resistance is reached) was calculated using the section moment W of the whole actual residual cross-section. Thereby, the W-values of the cuts (see Section 5.5.1) closest to failure zone, except for Beam 3, were used. For the Beam 3, the closest cut was noticeably different from failure zone and therefore values from another but more similar cut were used. Thus, depending on the specimen, a slight deviation from the exact value of the section moment W of the failure zone is possible.

A thickness of the zero strength layer d_0 is also presented in the results. The thickness was calculated as a comparison of cross-section dimensions of $b_{notional}$ and $h_{notional}$ of the cut with the same W value as actual residual cross-section (see Table 44) and the cross-section

dimensions needed if the bending strength were the same as in normal conditions; expected value in current case.

For comparative purposes, a prediction of the load bearing capacity for each test is given. The prediction was calculated according to the EC5 design rules. The dimensions of a theoretical notional cross-section at the time the fire resistance of the beam was reached were calculated considering a notional charring rate $\beta_n = 0,70$mm/min. Next, using the EC5 given zero strength value of 7mm, the height $h_{ef.EC5}$ and the width $b_{ef.EC5}$ of the effective cross-section were determined. The bending moment in fire $M_{fi.EC5}$ for this effective cross-section, assuming the material to have strength of normal temperature, is presented in the test result tables.

In order to illustrate the influence of local material properties, two extracts of the matrices are presented for each test. In the finger joint matrix, the locations marked with "1" the positions of a finger joint; whereas "0" means no finger joint. The other extract contains the values of the knot indicator K_m. The indicator K_m has been introduced in Section 4.1. For a short explanation, it can be said that the higher the number the bigger the knot. In both matrices, one cell contains information for a length of 1cm of one lamella. The matrices have been compiled and provided by Gerhard Fink.

Table 45. Overview of glulam beams' performance in fire tests.

Specimen	Strength class	Width (mid sect.)	Height (mid sect.)	Applied load level	Fire resistance	Mean charring rate	Type of failure	Location of failure, from ref. Point '0'	Zero strength layer, d_0
		[mm]	[mm]		[min:sec]	[mm/min]			[mm]
3	GL36h	158	256	0.2	68:53	0,682	CW	1585-1625	7,8
4	GL24h	158	253	0.3	48:06	0,804	CW+KC	1465-1495	4,4
5	GL36h	157	253	0.3	58:17	0,708	CW+KC	2200	1,5
6	GL36h	157	217	0.3	44:24	0,695	FJ+KC	1360	13,5

Abbreviations used in Table 43: FJ - finger joint, CW - clear wood, KC – knot cluster

5.5.2.1 Load bearing capacity of Beam "3"

The results of the fire test of Beam 3 with respect to the load bearing capacity are given in Table 46. In Graph 8, a load-displacement dependence is shown. Local weak sections as knot-indicator K_m values and locations of finger joints are introduced in Figure 73 and Figure 74, respectively.

In Figure 75, a failure location in the unburnt beam is shown and in Figure 76 the exact failure location before the fire test. Location of the failure reason, the finger joint, has been marked with red on the photograph. In Figure 80 the location of finger joint on the opposite side of the beam has been exhibited.

Failure of the Beam 3 may be called a mixed type; partly finger joint failure, partly clear wood failure. A deeper local charring zone in lamella 6 can be noted in Figure 77 on the right from the finger joint. As uneven charring created a significant deterioration on one side of the finger joint, tension in the lower part of finger joint remained unanswered as material's resistance to share is about ten times lower than tension along the grain, stresses in lamella were redistributed to only upper part of the finger joint. Redistribution resulted in failure. Clear wood failed of exceeding its shear capacity; note the shear cracks on the mid height of finger joint in Figure 77 and Figure 78. Figure 79 shows how lamellas have been torn apart in the location where tension should be transmitted to upper lamella.

Table 46. Test results with respect to load bearing of Beam 3.

Description	Abbr.	
Initial height [mm]	h	256
Initial width [mm]	b	158
Expected bending strength at normal temperature [MPa]	$f_{m,u,exp}$	39,8
Time in fire [min]	t	68:53
Prediction according to EC5 after time t in fire; β_n=0,7mm/min, d_0=7mm		
Notional effective height EC5 [mm]	$h_{ef.EC5}$	200,6
Notional effective width EC5 [mm]	$b_{ef.EC5}$	47,3
Bending moment bearing capacity after time t in fire [kNm]	$M_{fi.EC5}$	12,6
Experimental		
Residual notional charring rate [mm/min]	$\beta_{n.exp}$	0,67
Notional height [mm]	$h_{res.exp}$	209,6

Notional width [mm]	$b_{res.exp}$	65,2
Applied load level [-]		0,2
Bending moment at failure [kNm]	$M_{fi.exp}$	13,4
Location of failure, distance from "0" [mm]		1585
Type of failure, lamella "6"		CW+FJ
Type of failure, lamella "5"		CW
Bending stress at failure [MPa]	σ_m	28,0
Zero strength layer [mm]	d_0	7,8
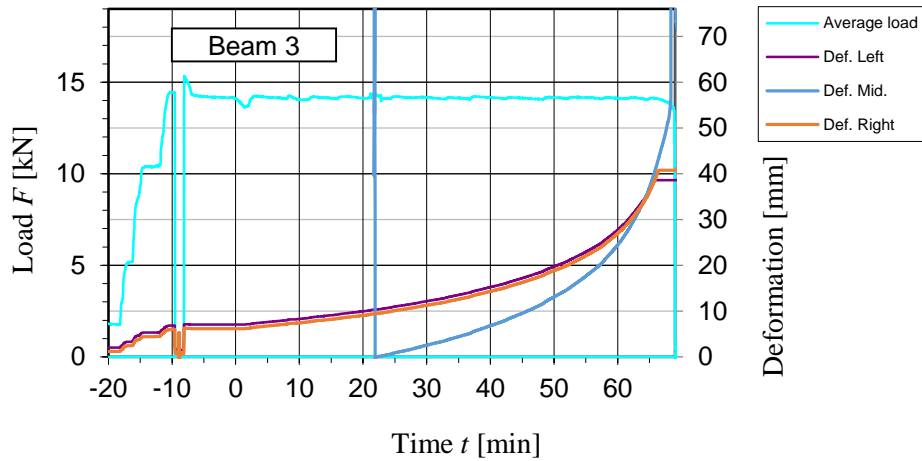
Graph 8. Average load and displacement measurements of fire test with Beam 3. Load F is the applied load per jack, as shown in Figure 32.
Note: Def. Mid. starts from 22-nd minute as "zero" and presents displacement since this moment of time.

1530	1540	1550	1560	1570	1580	1590	1600	1610	1620	1630
0	0	0	0	0	0	0	0	0	0	0
0	0	209	1198	1198	1198	1198	1198	1198	55	55
0	0	55	55	749	749	749	749	749	749	156
0	0	0	0	0	188	188	188	188	188	188
84	84	84	84	84	84	51	51	51	0	0
0	0	0	0	0	0	0	0	0	0	0
273	273	273	273	273	273	122	122	94	94	94

Figure 73. Extract of the K_m value matrix of the Beam 3.

1530	1540	1550	1560	1570	1580	1590	1600	1610	1620	1630
0	0	0	0	0	0	0	0	0	0	0
0	0	0	0	0	0	0	0	0	0	0
0	0	0	0	0	0	0	0	0	0	0
0	0	0	0	0	0	0	0	0	0	0
0	0	0	0	0	0	0	0	0	0	0
0	0	0	0	0	1	0	0	0	0	0
0	0	0	0	0	0	0	0	0	0	0

Figure 74. Extract of the finger joint location matrix of the beam 3.

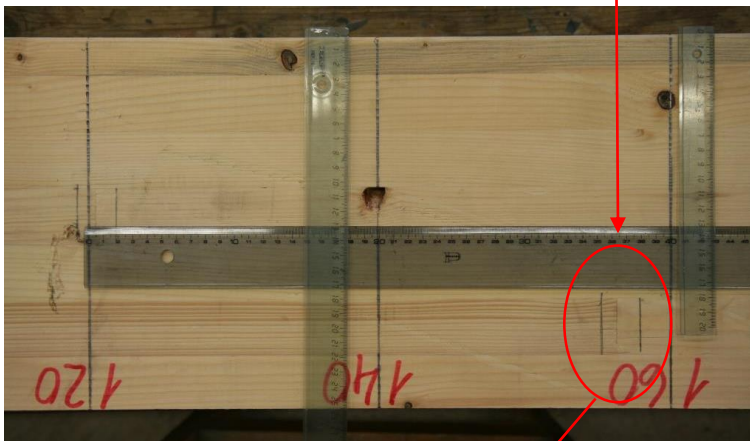*Figure 75. Position of Figure 76 on the Beam 3.*

Figure 76. Failure zone of Beam 3 face "D" before the fire test.
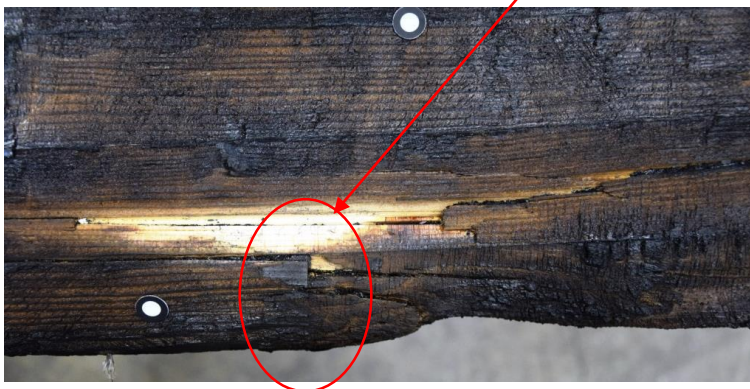

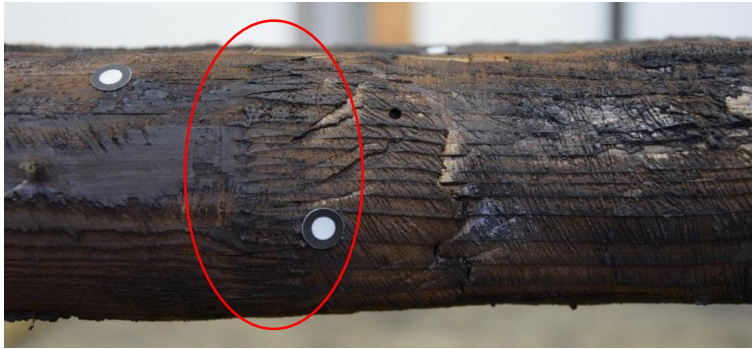*Figure 77. Failure zone of Beam 3 face "D" after the fire test.*

Figure 78. Bottom of the failure zone of Beam 3 after the fire test. Note the share failure on the right from finger joint.

Figure 79. Failure zone of Beam 3 face "B" after the fire test.

Figure 80. Failure zone of Beam 3 face "B" before the fire test.

5.5.2.2 Load bearing capacity of Beam "4"

The results of the fire test of Beam 4 with respect to the load bearing capacity are given in Table 47. In Graph 9, a load-displacement dependence and in Graph 10 the relative displacement of the mid-section are shown. Local weak sections as locations of finger joints and knot-indicator K_m values are introduced in Figure 81 and Figure 82, respectively. There is no finger joint in this failure zone.

In Figure 83, a failure location in the unburnt beam is shown and in Figure 84 the exact failure location before the fire test. Please note that in Figure 84 and in Figure 87 a knot cluster of extra high K_m value surrounded with red in Figure 82 is hardly noticeable on the unburnt specimen, which means that the knot is located in the middle of the lamella.

Failure of the Beam 4 can be called a mixed type; partly clear wood, partly a knot cluster. The bottommost lamella 6 has diminished about a half of its height because of charring and thus not enough of it is left to resist all the stress of tension zone, it is ruptured. Cracks of torn wood are visible in Figure 86. The reason why most of the tension was redistributed to lamella 6 is the knot presented in Figure 85 and its already mentioned high K_m value. Fact that the knot cluster of that size cannot be spotted on unburnt beam indicates that the deterioration of the structure of wood is larger deeper inside. In fire the visible undisturbed wood outside will char and the relative area of knot cluster is higher than before the test. Meaning, in this location lamella 5 in not able to reinforce adjacent lamella 6 at all and the latter will be torn.

Table 47. Test results with respect to load bearing of Beam 4.

Description	Abbr.	
Initial height [mm]	h	253
Initial width [mm]	b	158
Expected bending strength at normal temperature [MPa]	$f_{m,u,exp}$	31,2
Time in fire [min]	t	48:06
Prediction according to EC5 after time t in fire; β_n=0,7mm/min, d_0=7mm		
Notional effective height EC5 [mm]	$h_{ef.EC5}$	212,2
Notional effective width EC5 [mm]	$b_{ef.EC5}$	76,5

Bending moment bearing capacity after time t in fire [kNm]	$M_{fi.EC5}$	17,9

Experimental

Residual notional charring rate [mm/min]	$\beta_{n.exp}$	0,82
Notional height [mm]	$h_{res.exp}$	213,5
Notional width [mm]	$b_{res.exp}$	79,0
Applied load level [-]		0,3
Bending moment at failure [kNm]	$M_{fi.exp}$	16,0
Location of failure, distance from "0" [mm]		1465
Type of failure, lamella "6"		CW
Type of failure, lamella "5"		KC
Bending stress at failure [MPa]	σ_m	26,6
Zero strength layer [mm]	d_0	4,4
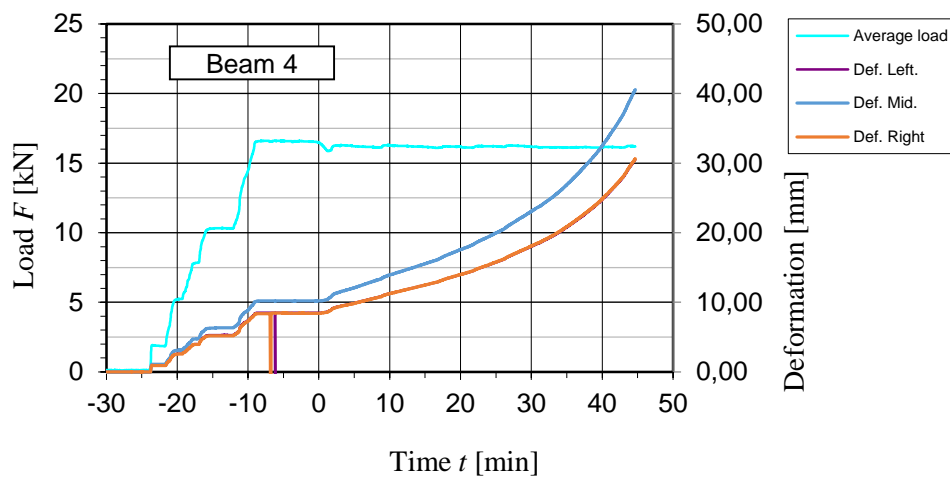
Graph 9. Average load and displacement measurements of fire test with Beam 4. Load F is the applied load per jack, as shown in Figure 32.
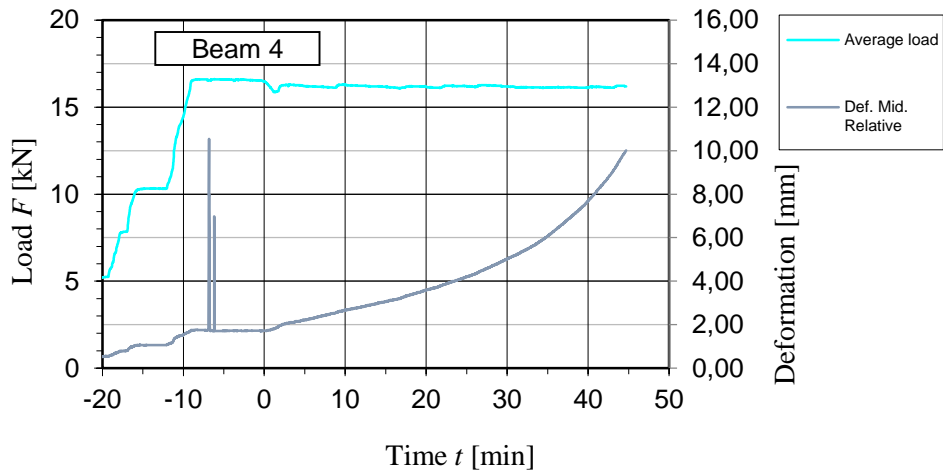
Graph 10. Relative deflection of the mid-span of Beam 4 between supports based on the measurements of all three LVDT-s. Load F is the applied load per jack, as shown in Figure 32.

1440	1450	1460	1470	1480	1490	1500	1510	1520	1530
0	0	0	0	0	0	0	0	0	0
0	0	0	0	0	0	0	0	0	0
0	0	0	0	0	0	0	0	0	0
0	0	0	0	0	0	0	0	0	0
0	0	0	0	0	0	0	0	0	0
0	0	0	0	0	0	0	0	0	0
0	0	0	0	0	0	0	0	0	0

Figure 81. Extract of the finger joint location matrix of the Beam 4.
No finger joints in failure zone.

1440	1450	1460	1470	1480	1490	1500	1510	1520	1530
430	434	1203	1203	1203	1203	1203	1203	0	0
0	0	0	0	0	0	0	0	0	85
0	0	0	0	0	0	0	0	0	0
4	4	4	1	1	1	0	0	0	0
23	98	210	3437	3437	3437	3437	3437	3437	207
0	0	0	0	0	0	0	0	0	0
0	0	0	0	0	0	0	0	4	25

Figure 82. Extract of the K_m value matrix of the Beam 4.

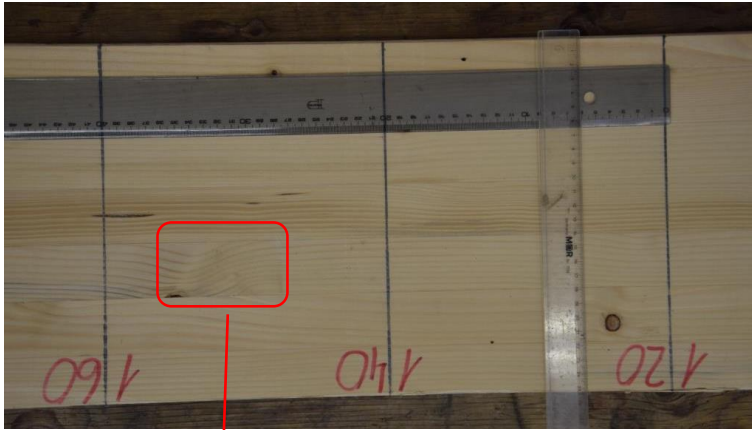*Figure 83. Position of Figure 84 on the Beam 4.*

Figure 84. Failure zone of Beam 4 face "B" before the fire test.
The red box indicates on the high Km value area marked in red in the lamella 5 in Figure 82.
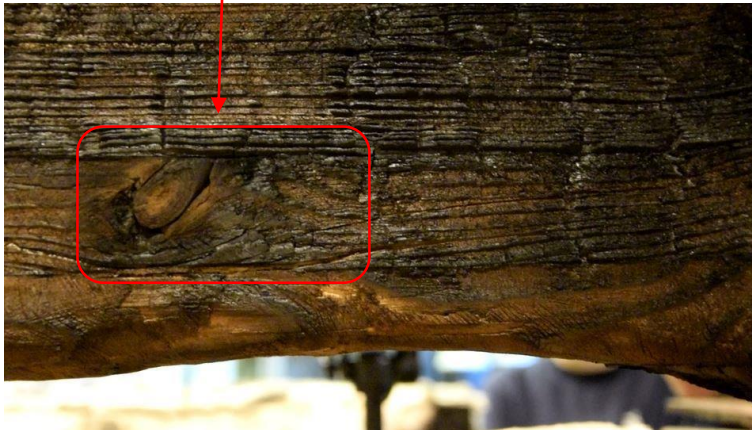

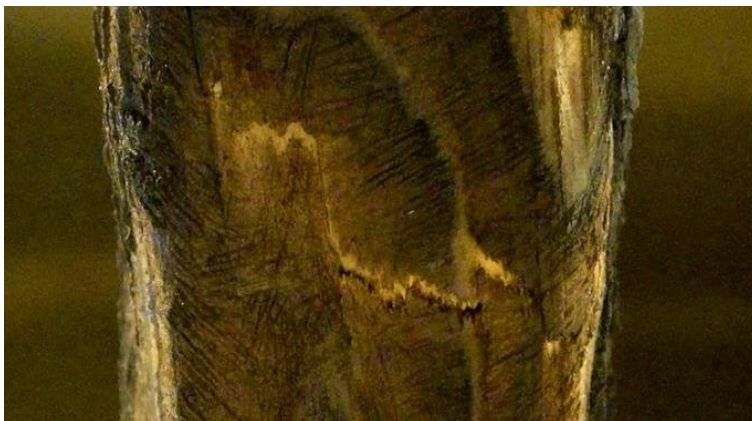*Figure 85. Failure zone of Beam 4 face "B" after the fire test.*

Figure 86. Bottom of the failure zone of Beam 4 after the fire test.

Figure 87. Failure zone of Beam 4 face "D" before the fire test. The red box marks high Km value in the matrix in Figure 82.

5.5.2.3 Load bearing capacity of Beam "5"

The results of the fire test of Beam 5 with respect to load bearing capacity are given in Table 48. In Graph 11, a load-displacement dependence and in Graph 12 the relative displacement of the mid-section are shown. Local weak sections as locations of finger joints and knot-indicator K_m values are introduced in Figure 88 and Figure 89, respectively. Three is no finger joint in this failure zone.

Beam 5 showed the longest fire resistance of the specimens of the same load level (0,3) which thus means it charred to a greater extent. The location of failure before the fire test is presented in Figure 91 on one side and in Figure 94 on the other side of the beam. The position of the failure zone in the unburnt specimen is shown in Figure 90. Causes of failure are similar to beam 4 – rupture of clear wood underneath a knot cluster of high K_m value; the upper lamella is not able to offer expected reinforcement to the bottommost one. Please see rupture cracks and knots on both sides of the burnt beam in Figure 92 in Figure 93. Please note in Figure 91 and Figure 94 that neither of the knots was visible from outside before the test.

Table 48. Test results with respect to load bearing of Beam 5.

Description	Abbr.	
Initial height [mm]	h	253
Initial width [mm]	b	157
Expected bending strength at normal temperature [MPa]	$f_{m,u,exp}$	39,8
Time in fire [min]	t	58:17
Prediction according to EC5 after time t in fire; β_n=0,7mm/min, d_0=7mm		
Notional effective height EC5 [mm]	$h_{ef.EC5}$	205,1
Notional effective width EC5 [mm]	$b_{ef.EC5}$	61,1
Bending moment bearing capacity after time t in fire [kNm]	$M_{fi.EC5}$	17,1
Experimental		
Residual notional charring rate [mm/min]	$\beta_{n.exp}$	0,71
Notional height [mm]	$h_{res.exp}$	211,7
Notional width [mm]	$b_{res.exp}$	74,5
Applied load level [-]		0,3
Bending moment at failure [kNm]	$M_{fi.exp}$	20,9

80

Location of failure, distance from "0" [mm]		2200
Type of failure, lamella "6"		CW
Type of failure, lamella "5"		KC
Bending stress at failure [MPa]	σ_m	37,6
Zero strength layer [mm]	d_0	1,5
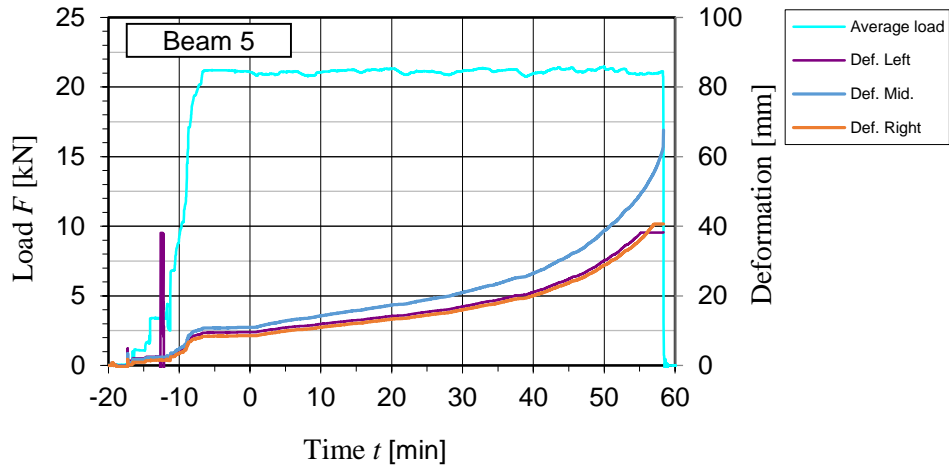
Graph 11. Average load and displacement measurements of fire test with Beam 5. Load F is the applied load per jack, as shown in Figure 32.
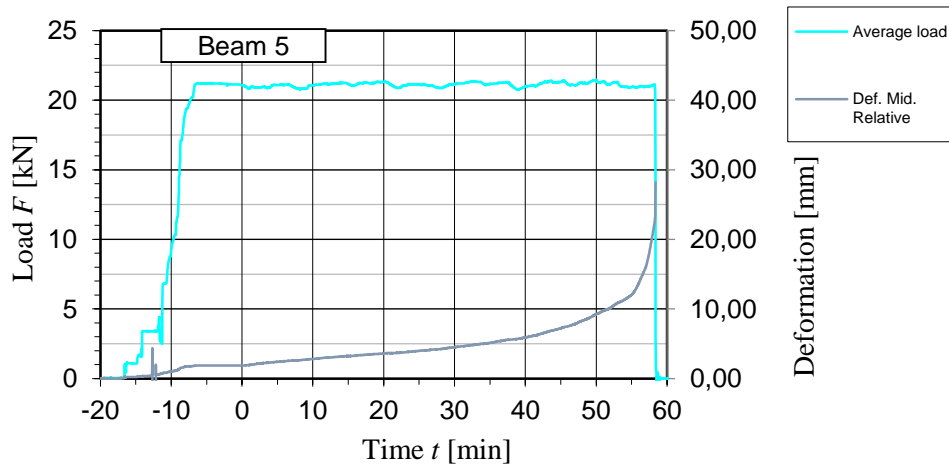
Graph 12. Relative deflection of the mid-span of Beam 5 between supports based on the measurements of all three LVDT-s. Load F is the applied load per jack, as shown in Figure 32.

2160	2170	2180	2190	2200	2210	2220	2230	2240	2250
0	0	0	0	0	0	0	0	0	0
0	0	0	0	0	0	0	0	0	0
0	0	0	0	0	0	0	0	0	0
0	0	0	0	0	0	0	0	0	0
0	0	0	0	0	0	0	0	0	0
0	0	0	0	0	0	0	0	0	0
0	0	0	0	0	0	0	0	0	0

Figure 88. Extract of the finger joint location matrix of the Beam 5.

2160	2170	2180	2190	2200	2210	2220	2230	2240	2250
1399	1399	1399	207	0	0	0	0	0	0
1331	61	30	0	0	0	0	0	0	0
275	275	275	275	2018	2018	2018	2018	2018	2018
0	0	0	0	0	0	0	0	147	147
0	6	6	1630	1630	1630	1630	1630	1630	168
0	6	6	0	0	0	0	0	0	0
0	0	0	0	0	0	0	0	0	0

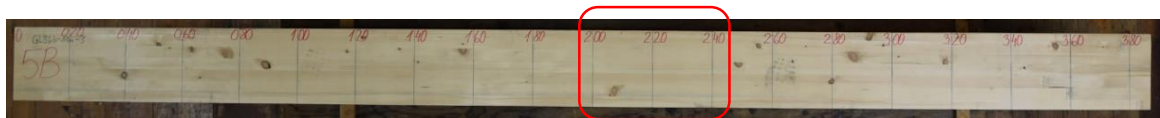*Figure 89. Extract of the K_m value matrix of the Beam 5.*

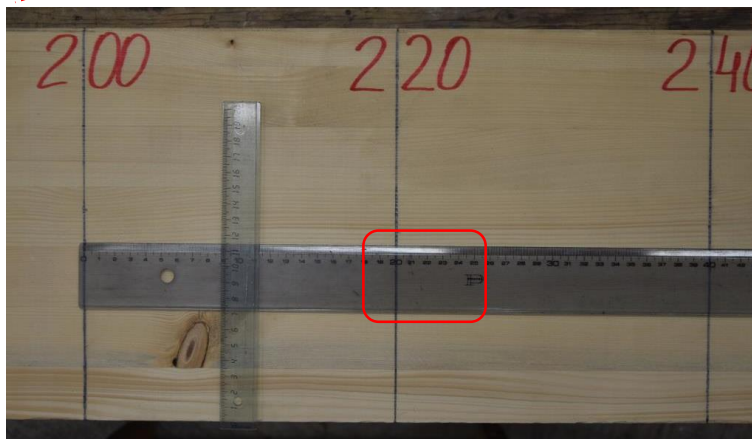*Figure 90. Position of Figure 91 on the beam 5.*

Figure 91. Failure zone of Beam 5 face "B" before the fire test. The red box marks a high K_m value zone in the lamella 5 in Figure 89.

Figure 92. Failure zone of Beam 5 face "B" after the fire test. Note the knot marked with red and clear wood rupture below it.
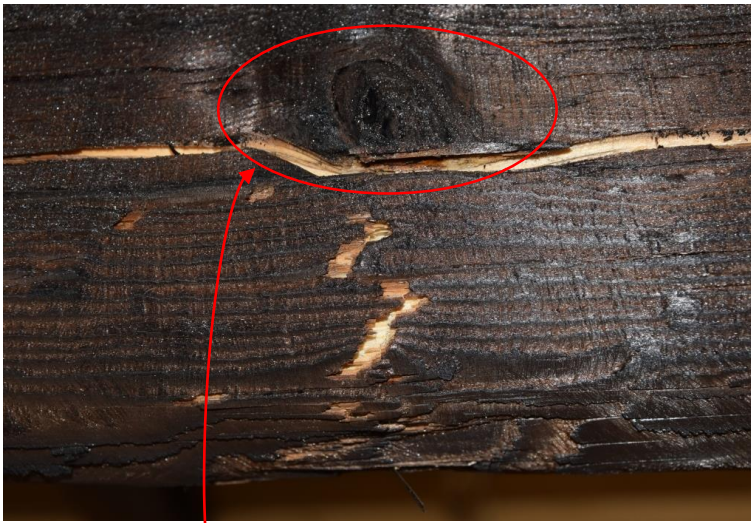

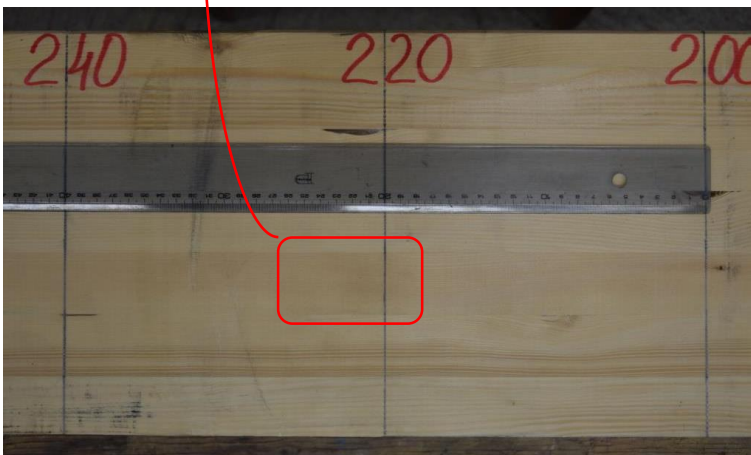*Figure 93. Failure zone of Beam 5 face "D" after the fire test.*

Figure 94. Failure zone of Beam 5 face "D" before the fire test. High knot indicator K_m zone marked in red.

5.5.2.4 Load bearing capacity of Beam "6"

The results of the fire test of Beam 6 with respect to the load bearing capacity are given in Table 49. In Graph 13, a load-displacement dependence and in Graph 14 relative displacement of the mid-section are shown. Local weak sections as locations of finger joints and knot-indicator K_m values are introduced in Figure 95 and in Figure 96, respectively.

The position of the failure zone in the unburnt specimen is exhibited in Figure 97. A closer overview of the failure zone is presented in Figure 98 and Figure 101. Note that knots are almost unnoticeable from the outside in the unburnt specimen. The main cause of failure is the finger joint (marked at 1360 in Figure 95) and the knot cluster just next to this finger joint located in the lamella above. An opened failed finger joint and cracked knot sections above it during the reloading process are presented in Figure 100 and Figure 101. Beam 6 failed either because the adjacent knot clusters were not able to reinforce weakened finger joint in the bottommost lamella or the other way around.

Table 49. Test results with respect to load bearing of Beam 6.

Description	Abbr.	
Initial height [mm]	h	217
Initial width [mm]	b	157
Expected bending strength at normal temperature [MPa]	$f_{m,u,exp}$	39,8
Time in fire [min]	t	44:24
Prediction according to EC5 after time t in fire; β_n=0,7mm/min, d_0=7mm		
Notional effective height EC5 [mm]	$h_{ef.EC5}$	178,8
Notional effective width EC5 [mm]	$b_{ef.EC5}$	80,7
Bending moment bearing capacity after time t in fire [kNm]	$M_{fi.EC5}$	17,1
Experimental		
Residual notional charring rate [mm/min]	$\beta_{n.exp}$	0,70
Notional height [mm]	$h_{res.exp}$	186,0
Notional width [mm]	$b_{res.exp}$	94,9
Applied load level [-]		0,3
Bending moment at failure [kNm]	$M_{fi.exp}$	14,2
Location of failure, distance from "0" [mm]		1360
Type of failure, lamella "5"		FJ
Type of failure, lamella "4"		KC
Type of failure, lamella "3"		KC
Bending stress at failure [MPa]	σ_m	24,9
Zero strength layer [mm]	d_0	13,5
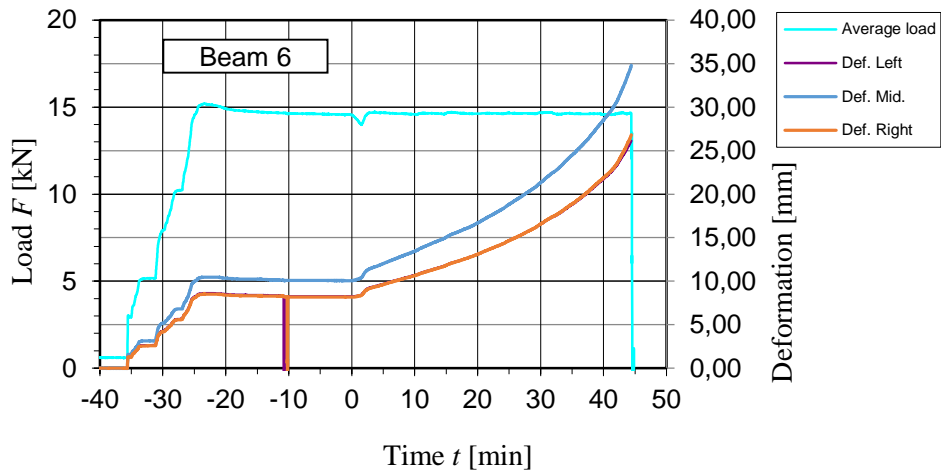
Graph 13. Average load and displacement measurements of fire test with Beam 6. Load F is the applied load per jack, as shown in Figure 32.
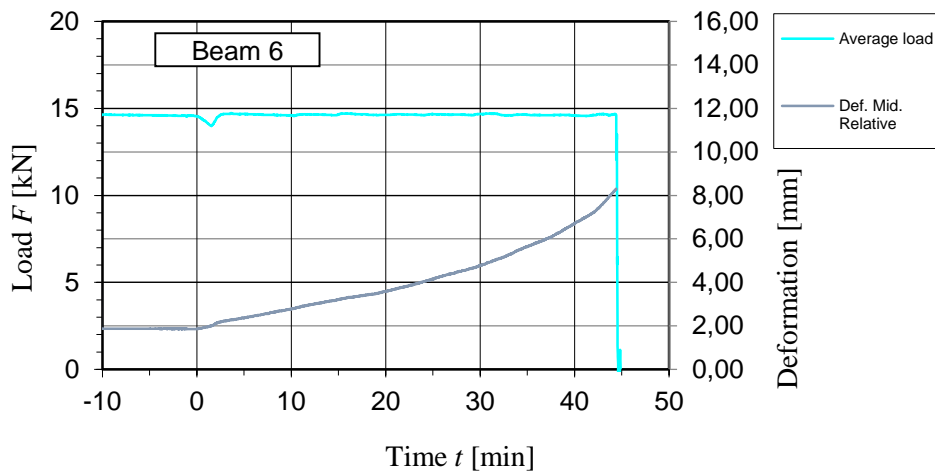
Graph 14. Relative deflection of the mid-span of Beam 6 between supports based on the measurements of all three LVDT-s. Load F is the applied load per jack, as shown in Figure 32.

1320	1330	1340	1350	1360	1370	1380	1390	1400	1410
0	0	0	0	0	0	0	0	0	0
0	0	0	0	0	0	0	0	0	0
0	0	0	0	0	0	0	0	0	0
0	0	0	0	0	0	0	0	0	0
0	0	0	0	1	0	0	0	0	0
0	0	0	0	0	0	0	0	0	0

Figure 95. Extract of the finger joint location matrix of the Beam 6.

1330	1340	1350	1360	1370	1380	1390	1400	1410	1420
81	81	0	0	0	0	0	0	0	0
0	0	0	0	0	0	0	3	32	108
16	16	16	93	963	963	963	963	963	963
0	0	6	43	117	1455	1455	1455	1455	1455
358	358	358	70	70	70	48	48	48	0
0	420	420	420	420	420	420	2	2	0

Figure 96. Extract of the K_m value matrix of the Beam 6.
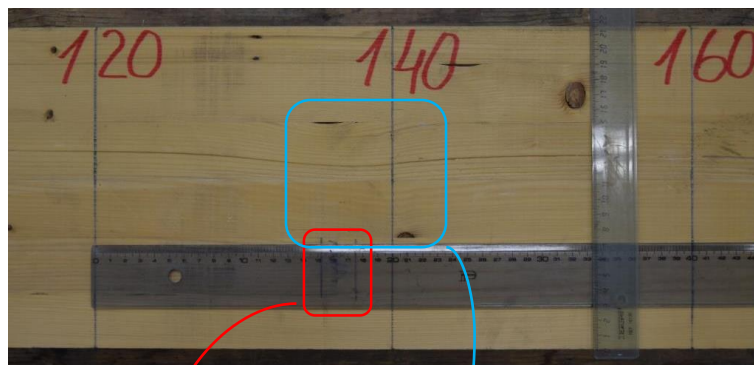

Figure 97. Position of Figure 98 on the Beam 6.

Figure 98. Failure zone of Beam 6 face "A" before the fire test. Red box marks finger joint and blue box a high Km values in the lamellas 3 and 4 in the Figure 96
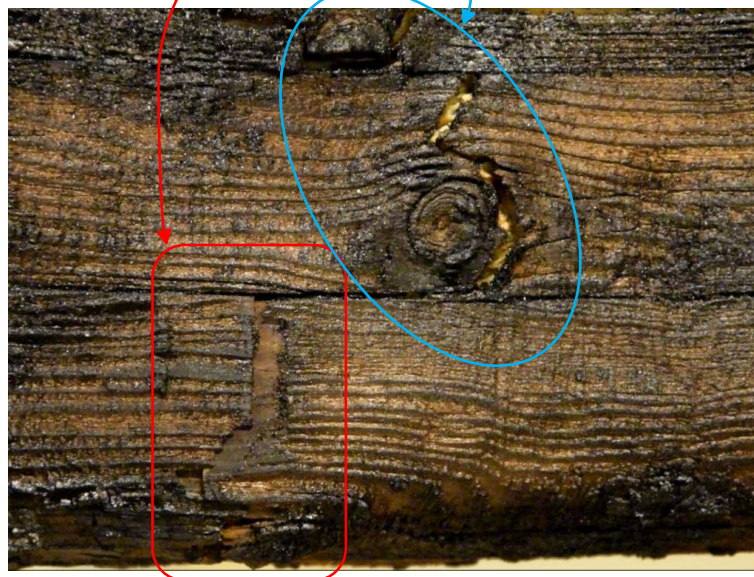

Figure 99. Failure zone of Beam 6 face "A" after the fire test.

Figure 100. Bottom of the failure zone of Beam 6 after the fire test. Note the fingers of the finger joint.

Figure 101. Failure zone of Beam 6 face "C" before the fire test. Finger joint location at 1360mm is marked with red.

6 Discussion

Charring

30 cuts of six different glued laminated timber beams which had been exposed to fire on three sides for different period of time were analysed in this thesis. Based on the moment of inertia of the actual residual cross-section, the equivalent notional charring rate β_n was calculated. Minimum and maximum values of all thirty cuts for the notional charring rate were 0,67 mm/min and 0,83 mm/min, respectively. Mean values of the specimen were between 0,68 mm/min and 0,80 mm/min. The mean value for β_n of all the cuts was 0,74 mm/min. As glulam beams consist of several different lamellas of naturally grown material of different properties uneven charring of the specimen could be expected. The highest coefficient of variation (COV) of the charring rate comparing cuts within specimen was 4,2% in the case of Beam 1, which was remarkably deformed. For the rest, COV remains under 2,5%. Differences between the specimens are higher and variation is described with a coefficient of 6,6%. In the current case, it can be pointed out that beams with noticeably smaller density charred quicker than the others. Objectively, six specimens are not a population for drawing conclusions. Further analysis of the data from already made experiments for finding possible correlations between different material properties and charring rate can be suggested.

Load bearing

Glulam beams with well-known local material properties had never been tested in fire before. The probabilistic approach of Fink [1] for modelling glulam beams which includes information from machine-grading of timber boards enabled a good overview of the weak sections of the beams.

Three main types of failure have been noted as the outcome of performed loaded fire tests: (1) Failure in finger joint, (2) failure in knot cluster and (3) failure of clear wood. However, failure of each beam included usually more than just one type. For example, as the bottommost lamella failed of clear wood tension, the next lamella above was described with

remarkably high K_m value in this location. Meaning the bottommost lamella of residual cross-section failed in the location where the second lamella from the bottom was not able to sustain the stresses because of a weak section and redistribution of stresses resulted the failure. A finger joint in the lowest lamella of the residual cross-section (finger joint in 2nd unburned lamella) led to failure of the beam in one fire test. This was also found in the PhD thesis of Klippel [21].

The size and distribution of weak sections inside a structural member is the matter of most importance. For each failure of the performed tests an easy explanation can be found in the matrices provided by Fink. Either a high knot-indicator value or a location of finger joint in certain lamella. Failure always involves a disturbance in clear, defect-free wood.

Based on the bending moment at failure and dimensions of the residual cross-section, the material bending strength was calculated for all specimens. Expectedly the values were remarkably lower than the expected value as strength properties decrease in elevated temperatures. Expected values for bending strength were 31,2 MPa for Beam 4 and 39,8 MPa for the other three beams. The bending stresses at failure were calculated as 26,6 MPa for Beam 4 and 28,0, 37,6 and 24,9 MPa for Beams 3, 5 and 6, respectively. Assuming the expected value to be actual strength of the material in normal conditions, the zero strength layer d_0 was calculated. The depth of the zero strength layer d_0 varied between 1,5 and 13,5 mm (for all values please see Section 5.5.2) while the number from current version of Eurocode 5 Part 1-2 is 7 mm. Comparing the stress and zero strength layer values from specimens 3,5 and 6, a noticeable deviation within a strength class can be noticed.

Looking at the load bearing predictions based on EC5 rules and expected material strength also given in the tables of results, on two occasions, Beam 3 (Table 46) and Beam 5 (Table 48), predicted moment bearing capacity was on the safe side, on the other two, Beam 4 (Table 47) and Beam 6 (Table 49) excessively optimistic.

7 Conclusions

In this study, loaded (4-point bending) fire tests with glulam beams with well-known local material properties were performed and in a subsequent step analysed The most significant aspects of the current study can be summarised as follows:

- The mean notional charring rate of rectangular glued laminated timber beams was with 0,74 mm/min on average slightly higher than the notional charring rate given in Eurocode 5 Part 1-2 for such elements (0,70 mm/min).

- The fire resistance of glulam beams from the same strength class can be significantly different due to local weak sections leading to early failure, as also found in the PhD thesis of Klippel [21].

- Based on four fire tests on glulam beams subjected to bending, a mean zero-strength layer was determined to 6,8 mm [min value: 1,5 mm; max value: 13,5 mm], which is in the range of the zero strength layer thickness according to Eurocode 5, Part 1-2 (7 mm). However, obviously the number of fire tests is very low.

- This report provides extensive input data to be further analysed within a comprehensive research project with the title "Reliability based design of timber in fire" at ETH Zürich.

8 Outlook

The main goal of this study was to collect data of the fire behaviour of in bending loaded glued laminated timber beams with well-known local material properties. All data gained from the performed fire tests will be imitated in computer simulations at ETH Zürich. The results of this thesis with respect to load bearing capacity will be a valuable comparison for the simulations.

Further, the following evaluation of the fire tests could be performed:

- Analysis of charring for each lamella and connect this information with the known material properties (e.g. density) for each lamella
- Verification of the 3D-scanned residual cross-section with the cuts presented in this thesis
- Development of a probabilistic charring model on the basis of the information presented in this thesis and the well-known material properties of timber coming from Fink's model
- Analysis of the change of timber's stiffness properties when exposed to fire
- Determination of the change of timber's strength properties when exposed to fire and comparison to the EC5 approach

Kokkuvõte

Puitmaterjalide kasutamine ehituskonstruktsioonides on märgatavalt laienenud viimastel aastakümnetel, puudutades mitte ainult väikeelamuid, vaid ka korrusmaju ning tööstus- ja ühiskondlikke hooneid. Uute materjalide kasutuselevõtt on tugevalt kasvatanud ambitsioone puidupõhistest materjalidest kõrghoonete püstitamiseks, millistes tuleohutuse osa projekteerimisprotsessis muutub märgatavalt kriitilisemaks.

Aastal 2014, kaitses Fink (ETH Zürich) doktoritöö liimpuittalade tugevuse tõenäosuspõhise mudeli arendamisest ning kohandamisest masinsorteerimisel automaatselt mõõdetavatele teguritele. Selle uurimuse katsekehad lõigati välja esialgsetest suurematest liimpuittaladest, mida kasutati Stadelmanni (ETH Zürich) magistritöö raames Finki mudeli valideerimiseks ning transporditi SP uurimisinstituuti Stockholmis.

Käesoleva töö käigus inspekteeriti põhjalikult kõik 6 tala võimalike kahjustuste osas ning nende füüsikalised näitajad dokumenteeriti. Viis tala koormati püsiva paindemomendiga, mis vastab 0,3-kordsele purustavale momendile normaaltingimustel, kuni purunemiseni tules. Taladest üks koormati püsiva 0,2-kordse normaaltugevuse momendiga ning sellesse paigaldati traat-termopaarid jälgimaks temperatuurijaotust katsekeha sees.

Tulekatsete järgselt kõik talad puhastati, purunemiste asukohad ja tüübid dokumenteeriti. Iga katsekeha lõigati viiest asukohast põlenud tsoonis sammuga 200mm. Põlenud tsooni jääkristlõiked fotografeeriti, nende perimeeter jäljendati vektorgraafikas. Tehtud lõikeid analüüsiti tingliku söestumise osas ning võrreldi kehtiva Eurokoodeks 5 osa 1-2 (EC5) versiooniga. Keskmine tinglik söestumine saadi katsete tulemusel pisut kõrgem ($\beta_{n,exp} = $ 0,74mm/min) kui EC5 poolt määratud väärtus (0,7mm/min). Samast tugevusklassist talade tulepüsivus võib olla oluliselt erinev kohalike nõrgestuste tõttu, nagu näiteks sõrmjätkud ja oksakohad, ning viia varase purunemiseni. Põhinedes neljale katsele, millistes hinnati kandevõimet, leiti keskmiseks null-tugevusega kihi d_0 paksuseks 6,8mm, mis on võrreldav kehtiva EC5 antava suurusega (7mm). Siiski, katsete arv oli liialt väike järeldusteks.

See töö annab olulisel hulgal sisendinformatsiooni edasisteks analüüsideks laiaulatuslikus uurimustöös pealkirjaga „Tõenäosuslikkusel põhinev puitkonstruktsioonide projekteerimine tuleolukorras".

References

[1]   Fink, G. "Influence of varying material properties on the load-bearing capacity of glued laminated timber." PhD thesis, Diss., Eidgenössische Technische Hochschule ETH Zürich, Nr. 21746, 2014

[2]   Norén J., "Failure of Structural Timber when Exposed to Fire. Part 2", Swedish Institute for Wood Technology Research, Report No. 8810066. Stockholm, 1988.

[3]   European Committee for Standardization, "EN 1995-1-2, Eurocode 5: Design of Timber Structures - Part 1-2: General - Structural fire design," Brussels, 2004.

[4]   Madsen B. & et al. "Structural behavior of timber". Timber Engineering Ltd, 1992.

[5]   Just E.-J., Paindekatsed , TTÜ, 2004

[6]   Niemz P., "Physik des Holzes". Tech. rep., Institut für Baustoffe, ETH Zürich, Switzerland, 2005.

[7]   Kollmann F.F.P., Cote Jr W.A. & et al. "Principles of wood science and technology. I. Solid wood." George Allen & Unwin Ltd., 1968.

[8]   Harris J.M., "Spiral Grain and Wave Phenomena in Wood Formation." Springer, Berlin Heidelberg, 1989.

[9]   Gerhards C.C., "Effect of slope of grain on tensile strength." Forest Products Journal 38(7/8):39-40, 1988.

[10] Ormarsson S., Dahlblom O. & Persson K., "Influence of varying growth characteristics of stiffness grading of structural timber." In: Proceedings of the 44th Meeting, International Council for Research and Innovation in Building and Construction, Working Commission W18 - Timber Structures, Savonlinna, Finland, CIB-W18, Paper No. 31-5-1, 1998.

[11] Pope D., Marcroft J. & Whale L., "The effect of global slope of grain on the bending strength of scaffold boards." Holz als Roh-und Werkstoff 63(5):321-326, 2005.

[12] Fink G., Kohler J. & Frangi A., "Experimental Analysis of the Deformation and Failure Behaviour of Significant Knot Clusters.", In: Quenneville P. (ed) World Conference on Timber Engineering 2012 (WCTE 2012) : The Future of Timber Engineering : Auckland, New Zealand : 15-19 July 2012. Volume 1, Curran Associates, Inc., Red Hook, NY, pp 270-279, 2012.

[13] Falk R.H. & Colling F., "Laminating effects in glued-laminated timber beams.", Journal of structural engineering 121(12):1857-1863, 1995.

[14] Serrano E. & Larsen H.J., "Numerical investigations of the laminating effect in laminated beams.", Journal of Structural Engineering 125(7):740-745, 1999.

[15] Ehlbeck J., Colling F. & Görlacher R., "Einfluβ keilgezinkter Lamellen auf die Biegefestigkeit von Brettschichtholzträgern.", European Journal of Wood and Wood Products 43(8):367-373, 1985.

[16] Heimeshoff B. & Glos P., "Zugfestigkeit und Biege-E-Modul von Fichten-Brettlamellen." , European Journal of Wood and Wood Products 38(2):51-59, 1980.

[17] Colling F., "Tragfähigkeit von Biegeträgern aus Brettschichtholz in Abhängigkeit von den festigkeitsrelevanten Einussgröβen.", Versuchsanstalt für Stahl, Holz und Steine, Karlsruhe, Germany, 1990.

[18] Schickhofer G., "Development of eficient glued laminated timber. In: Proceedings of the 29th Meeting, International Council for Research and Innovation in Building and Construction, Working Commission W18 - Timber Structures, Bordeaux, France, CIB-W18, Paper No. 29-12-1, 1996.

[19] König J., "Structural fire design according to Eurocode 5 - design rules and their background.", Fire and Materials 29(3):147–163, 2005.

[20] ISO 834-1 Fire resistance tests – Elements of building construction – Part 1: General requirements. International Organization of Standardization, Genève, Switzerland, 1999.

[21] Klippel M., "Fire safety of bonded structural timber elements.", PhD thesis, ETH No. 21843; ETH Zurich, Zurich, Switzerland, 2014.

[22] Schmid J., Klippel M., Just A., Frangi A., "Comparison of the fire resistance of timber members in tests and calculation models", CIB-W18 Meeting 46 - 26 August to 29 August 2012 – Vancouver, Canada, SP Technical Research Institute of Sweden, ETH Zürich, Institute of Structural Engineering IBK, Zürich, Switzerland, 2012.

[23] CEN, "EN 338: Structural timber – Strength classes.", European Committee for Standardization, Brussels, Belgium, 2009b

[24] Klippel, M., Frangi, A., "Fire tests on finger-jointed timber boards - Test report"; IBK report No. 354, ETH Zurich, Zurich, Switzerland, 2014.

[25] Philipp Stadelmann, "Experimental investigations to evaluate the load-bearing behaviour of glued laminated timber with well-known beam setup", Master Thesis, Zürich, 2015

[26] Isaksson T., "Modelling the variability of bending strength in structural timber." PhD thesis, Lund Institute of Technology, Lund, Sweden, 1999.

[27] https://www.digchip.com/datasheets/parts/datasheet/3375/HS50.php

Annexes

Annex A. Overview photographs of the specimens

A.1 Overview photographs of specimen 1

*Figure 105.
Specimen 1,
Face "A"*

*Figure 104.
Specimen 1,
Face "B"*

*Figure 103.
Specimen 1,
Face "C"*

*Figure 102.
Specimen 1,
Face "D"*

A.2 Overview photographs of specimen 2

*Figure 109.
Specimen 2,
Face "A"*

*Figure 108.
Specimen 2,
Face "B"*

*Figure 107.
Specimen 2,
Face "C"*

*Figure 106.
Specimen 2,
Face "D"*

A.3 Overview photographs of specimen 3

Figure 110. Specimen 3, Face "A"

Figure 112. Specimen 3, Face "B"

Figure 111. Specimen 3, Face "C"

Figure 113. Specimen 3, Face "D"

A.4 Overview photographs of specimen 4

*Figure 117.
Specimen 4,
Face "A"*

*Figure 115.
Specimen 4,
Face "A"*

*Figure 116.
Specimen 4,
Face "A"*

*Figure 114.
Specimen 4,
Face "A"*

A.5 Overview photographs of specimen 5

Figure 121. Specimen 5, Face "A"

Figure 120. Specimen 5, Face "A"

Figure 119. Specimen 5, Face "A"

Figure 118. Specimen 5, Face "A"

A.6 Overview photographs of specimen 6

Figure 123. Specimen 6, Face "A"

Figure 124. Specimen 6, Face "B"

Figure 125. Specimen 6, Face "C"

Figure 122. Specimen 6, Face "D"